

(12)

LEVEL III

AD-E 300 656

DNA 4831F

# STRESS PULSE TAIL EXPERIMENTS WITH ELECTRON BEAMS AND UNDERGROUND TEST

Ktech Corporation  
901 Pennsylvania Ave., N.E.  
Albuquerque, New Mexico 87110

30 January 1979

Final Report for Period 5 July 1977-31 October 1978

CONTRACT No. DNA 001-77-C-0292

ADA080550

DDC FILE COPY

APPROVED FOR PUBLIC RELEASE;  
DISTRIBUTION UNLIMITED.

THIS WORK SPONSORED BY THE DEFENSE NUCLEAR AGENCY  
UNDER RDT&E RMSS CODE B342078462 J11AAXAX00234 H2690D.

Prepared for  
Director  
DEFENSE NUCLEAR AGENCY  
Washington, D. C. 20305

DDC  
RECEIVED  
FEB 13 1980  
B

80- 4 1 026

Destroy this report when it is no longer  
needed. Do not return to sender.

PLEASE NOTIFY THE DEFENSE NUCLEAR AGENCY,  
ATTN: STTI, WASHINGTON, D.C. 20305, IF  
YOUR ADDRESS IS INCORRECT, IF YOU WISH TO  
BE DELETED FROM THE DISTRIBUTION LIST, OR  
IF THE ADDRESSEE IS NO LONGER EMPLOYED BY  
YOUR ORGANIZATION.



UNCLASSIFIED

SECURITY CLASSIFICATION OF THIS PAGE (When Data Entered)

REPORT DOCUMENTATION PAGE		READ INSTRUCTIONS BEFORE COMPLETING FORM
1. REPORT NUMBER DNA 4831F	2. GOVT ACCESSION NO.	3. RECIPIENT'S CATALOG NUMBER
4. TITLE (and Subtitle) STRESS PULSE TAIL EXPERIMENTS WITH ELECTRON BEAMS AND UNDERGROUND TEST		5. TYPE OF REPORT & PERIOD COVERED Final Report for Period 5 Jul 77-31 Oct 78
7. AUTHOR(s) Dr. Donald V. Keller David A. Rice		6. PERFORMING ORG. REPORT NUMBER TR79-1
9. PERFORMING ORGANIZATION NAME AND ADDRESS Ktech Corporation 901 Pennsylvania Avenue, NE Albuquerque, New Mexico 87110		8. CONTRACT OR GRANT NUMBER(s) DNA 001-77-C-0292
11. CONTROLLING OFFICE NAME AND ADDRESS Director Defense Nuclear Agency Washington, D.C. 20305		10. PROGRAM ELEMENT, PROJECT, TASK AREA & WORK UNIT NUMBERS NWED Subtask J11AAXAX002-34
14. MONITORING AGENCY NAME & ADDRESS (if different from Controlling Office) 12) 63		12. REPORT DATE 30 Jan 79
		13. NUMBER OF PAGES 62
16. DISTRIBUTION STATEMENT (of this Report) Approved for public release; distribution unlimited.		15. SECURITY CLASS (of this report) UNCLASSIFIED
17. DISTRIBUTION STATEMENT (of the abstract entered in Block 20, if different from Report) 18) DNA, SBIE 19) 4831F, AD-E 300 656		15a. DECLASSIFICATION/DOWNGRADING SCHEDULE
18. SUPPLEMENTARY NOTES This work sponsored by the Defense Nuclear Agency under RDT&E RMSS Code B342078462 J11AAXAX00234 H2590D.		
19. KEY WORDS (Continue on reverse side if necessary and identify by block number) Pressure Pulse Tail Blow-off Impulse Split-Hopkinson Bar Charge-Mode Piezoelectric Transducers		
20. ABSTRACT (Continue on reverse side if necessary and identify by block number) The Split-Hopkinson bar technique has been used to study the late time stress amplitude from blow-off of quartz phenolic, tape wrapped carbon phenolic, and phenolic resin by pulsed electron beams and underground test irradiation. In all cases, the stress decreased to less than 10 bars within 10 to 20 $\mu$ s after the main stress peak. There is no late time stress of sufficient amplitude to significantly affect material or structural response. This result indicates that the prompt impulse, not total impulse, should be used for		

DD FORM 1 JAN 73 1473 EDITION OF 1 NOV 65 IS OBSOLETE

UNCLASSIFIED

SECURITY CLASSIFICATION OF THIS PAGE (When Data Entered)

408 270

UNCLASSIFIED

SECURITY CLASSIFICATION OF THIS PAGE(When Data Entered)

20. ABSTRACT (Continued)

calculations, correlations and above ground simulations. The thin piezo-electric crystal was also used in a new gauge design (CMX gauge) for long time stress recording in one-dimensional strain geometry with high frequency response and very high stress sensitivity. The one-dimensional read time is limited only by the size of the irradiated area. The gauge was tested with simultaneous laser velocity interferometer measurements. The limited data obtained with the CMX gauge indicated that the stress history is recorded in detail permitting integration to determine the impulse generation as a function of time.

UNCLASSIFIED

SECURITY CLASSIFICATION OF THIS PAGE(When Data Entered)

## SUMMARY

The major accomplishments of this program may be summarized as follows:

1. The Split-Hopkinson bar technique has been used successfully with both pulsed electron-beam and underground tests to study the stress history from blow-off of quartz phenolic, tape-wrapped carbon phenolic, and phenolic resin.
2. The late-time stress tail following the main blow-off pulse was shown to fall below 10 bars with 10 to 20  $\mu$ s for all three materials when subjected to the electron-beam irradiations. There is no late time stress of sufficient amplitude to significantly affect either material or structural responses.
3. Radial oscillations of the SHB rod, although fully understood and amenable to calculation, limit the stress resolution in the pulse tail to a few percent of the main pulse amplitude (i.e., a few bars). The time resolution of the SHB is a few microseconds, so that high frequency details of the main blow-off stress pulse are lost; however, since the axial momentum is conserved the SHB is a highly reliable means of determining the prompt impulse.
4. The SHB was used successfully in an underground test. Very low noise levels were achieved by the use of differential operation with signal conditioning electronics and a crow-bar circuit. The measured (prompt) impulse agreed well with calculations, and with separate total impulse measurements.
5. The thin piezoelectric quartz crystal has been used very successfully in a one-dimensional strain geometry (termed the CMX gauge). This new gauge design combines the high frequency response ( $\leq 20$  ns) of conventional stress gauges with the great stress sensitivity ( $\leq 1$  bar) of the charge-mode operation used in the SHB. Data taken with this new gauge agree with laser interferometry. The one-dimensional reading time is limited only by the size the irradiated area.

ACCESSION for		
NTIS	White Section	<input checked="checked" type="checkbox"/>
DDC	Buff Section	<input type="checkbox"/>
UNANNOUNCED		<input type="checkbox"/>
JUSTIFICATION		
BY		
DISTRIBUTION/AVAILABILITY CODES		
Dist.	AVAIL.	and/or SPECIAL
A		

The results showed that only the prompt impulse (within 5 to 10  $\mu$ s) has associated stresses of sufficient amplitude to affect either material or structural response. Measured total impulses have been used almost exclusively in the past to correlate with material and structural damage and the total impulses are 50 to 100 percent greater than the prompt impulse (obtained with stress gauges reading for 1-2  $\mu$ s). It is not surprising that the past correlations have not been very successful. Also, the total impulse has been used to define loading conditions for aboveground simulation testing (magnetic flyers and explosives), and to infer parameters for impulse calculations (e.g., effective sublimation or melt energies for the BBAY and MBBAY models). It would now appear that prompt impulse should be used to define model parameters and simulations tests. The phenomena responsible for the late time impulse (exothermic vapor decomposition, or whatever) are probably not important to damage mechanisms.

It is therefore important to establish the prompt impulse (defined as that delivered over the time until the stress falls to a few bars) for phenolic resin, and important phenolic resin composites (TWCP and QP) for several electron beam and UGT spectra and fluences, and to use this data to reexamine the predictive capabilities of the analytic and hydrodynamic impulse and damage models. We now have the capabilities (SHB and CMX gauges, and large area electron beams) that make this a straightforward study.

Specific recommendations are:

1. Develop the instrumentation to enable SHB and CMX measurements to be made simultaneously with the total impulse. The SHB could be incorporated into a ballistic pendulum, and the CMX into a modified LVT, TRIM or other gauge.
2. Measure prompt and total impulses simultaneously for phenolic resin, QP and CP for two or more electron beam spectra as a function of fluence.
3. For the above materials, measure the blow-off stress histories, using the CMX gauge, until the stress falls to near 1 bar. Correlate these stresses and impulses with PUFF, TINC and MBBAY models. Determine the applicability of past model parameters, correlations and predictions.

## PREFACE

The authors express their appreciation to the following individuals for helping make this program a success: Mr. Robert Mason, Ktech Corporation, for performing various calculations; Lt Irving Copus, Air Force Weapons Laboratory (DYV), Kirtland Air Force Base, NM for performing energy deposition and PUFF hydrodynamic calculations; Messrs. Joe Smith and Jim Spates, Ktech, for design, assembly and testing of the coaxial line driver and crow-bar electronics; Mr. Tony Robinson, Naval Research Laboratories, Washington, D. C., for the operation of the GAMBLE I generator; Messrs. H. Woodall and T. Lynch, Sandia Laboratories for the operation of REHYD; and, Messrs. Dave Phelps and Joe Devlin for operation of Blackjack 3.

# TABLE OF CONTENTS

<u>Section</u>		<u>Page</u>
1	INTRODUCTION-----	7
2	PROGRAM OBJECTIVES	
	2.1 SHB Electron-beam Tests-----	12
	2.2 One-Dimensional Piezoelectric Gauge Development-----	12
	2.3 SHB Diablo Hawk Tests-----	12
3	ELECTRON BEAM MACHINES	
	3.1 Description-----	13
	3.2 GAMBLE I Accelerator-----	13
	3.3 REHYD Accelerator-----	16
	3.4 Blackjack 3 Accelerator-----	16
	3.5 Beam Diagnostics-----	20
4	CALCULATIONS	
	4.1 Deposition Profile-----	21
	4.2 Impulse-----	22
	4.3 Stress Wave Calculations-----	22
	4.3.1 One-Dimensional Calculations-----	22
	4.3.2 Two-Dimensional Calculations-----	23
5	EXPERIMENT DESIGN CONSIDERATIONS	
	5.1 Split-Hopkinson (SHB) Design-----	26
	5.1.1 Bar Design-----	26
	5.1.2 Collimator-----	29
	5.1.3 Cassette Design-----	31
	5.1.4 Signal Conditioning Electronics-----	32
	5.1.5 SHB Calibration-----	34
	5.2 One-Dimensional Piezoelectric Gauge-CMX Gauge-----	34
6	RESULTS	
	6.1 Electron-Beam Results with SHB-----	38
	6.1.1 Noise Level-----	38
	6.1.2 3DQP Results-----	39
	6.1.3 TWCP Results-----	41
	6.1.4 Phenolic Resin-----	41
	6.1.5 Tamped and Long Duration Stresses-----	44
	6.2 One-Dimensional CMX Gauge Results-----	45
	6.3 Discussion of Preliminary Underground SHB Test Results -	50
7	REFERENCES-----	56

# LIST OF FIGURES

<u>Figure</u>		<u>Page</u>
1	Split Hopkinson (SHB) and Crystal Configuration.-----	8
2	Decomposition of Stress Pulse Into Main Pulse Plus Pulse Tail--Propagation and Attenuation in Rods.-----	10
3	Sketch of Diode and Experiment Geometry for GAMBLE I.-----	14
4	Normalized Depth-dose Profiles for GAMBLE I, Blackjack 3, and REHYD.-----	15
5	Photograph of REHYD Diode.-----	17
6	Radial Distribution of Fluence for Blackjack 3 and REHYD.-----	18
7	Sketch of Diode and Experiment Geometry for Blackjack 3.---	19
8	Calculated Stress Attenuation Versus Distance for GAMBLE I.-----	24
9	Cassette Design for Ktech Split Hopkinson Bar Experiments.-	28
10	SHB Collimator for Underground Test Application.-----	30
11	Simplified Schematic for SHB and Signal Conditioning Electronics.-----	33
12	Sketch of One-dimensional Charge Mode Crystal Gauge-CMX.---	36
13	Photograph of CMX Gauge Assembly with a Quartz Phenolic Target Backed by Plexiglas Used in Shot No. 2122.-----	37
14	SHB Noise Test. GAMBLE I Shot No. 6040.-----	39
15	SHB Result for 3DQP. GAMBLE I Shot No. 6042.-----	40
16	SHB Result for TWCP. Blackjack 3 Shot No. 2164.-----	42
17	SHB Result for Phenolic Resin. GAMBLE I Shot No. 6046.----	43
18	SHB Result for Partially Tamped 3DQP. GAMBLE I Shot No. 6057.-----	44
19	SHB Measurement of Long Low Stress from Anode Debris. GAMBLE I Shot No. 6063.-----	45
20	CMX Result on 3DQP. REHYD Shot No. 2122. Laser Inter- ferometer Result and PUFF Hydrocode Calculation Shown for Comparison.-----	47
21	CMX Result on 3DQP. REHYD Shot No. 2122.-----	48
22	Photograph of Irradiated Quartz Phenolic Target Showing Non-uniform Blow-off. Blackjack 3 Shot No. 2122.-----	49
23	SHB Results from Underground Test: (a) Active and (b) Background Results.-----	51

# LIST OF FIGURES (continued)

<u>Figure</u>		<u>Page</u>
24	SHB Results from Underground Test. Comparison of (a) Active, and (b) Background Results.-----	52
25	SHB Stress Pulse for 3DQP from Underground Test and Comparison With Two-dimensional Hydrodynamic Calculation.-----	54

## LIST OF TABLES

<u>Table</u>		
1	Electrical Characteristics of GAMBLE I, Blackjack 3 and REHYD.-----	16
2	3DQP Impulse Calculations.-----	22
3	TOODY Calculation.-----	25
4	Piezoelectric Sensitivity for X-cut Quartz and Lithium Niobate.-----	31

## SECTION 1

### INTRODUCTION

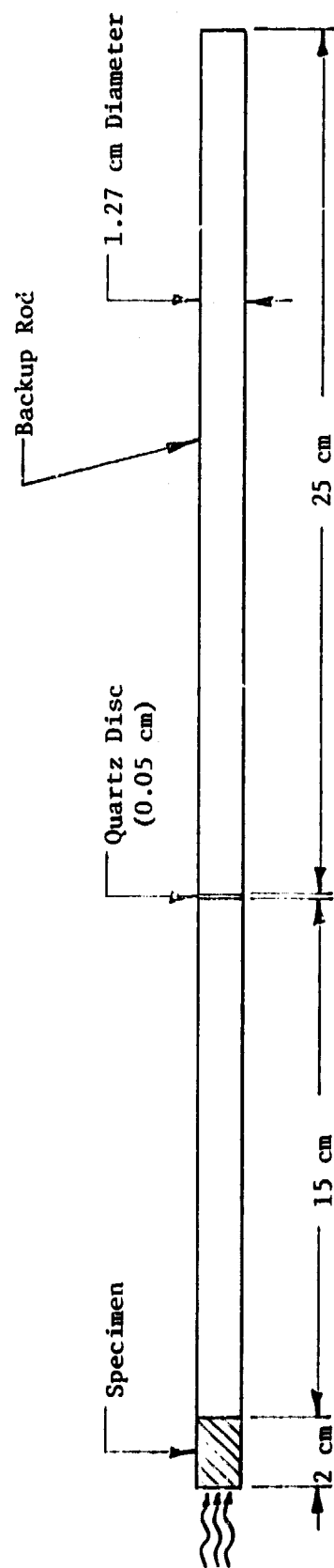
The total blow-off impulse, recorded by slow response gauges (e.g., LVT, cut-wire, etc.) is typically 50 to 100 percent more than the time integral of stress waves recorded for 1 to 2 microseconds with fast stress gauges (e.g., X-cut quartz and carbon). It is important to resolve the origin of the later time ( $> 2\mu\text{s}$ ) portion of the impulse by determining the entire stress history.

The amplitude and duration of the late time stress, following the main stress pulse, must be determined to properly determine the loading for structural response analyses or simulations. Thus, the entire stress pulse must be followed (i) until the stress amplitude falls below levels of structural interest (10 to 100 bars, depending upon the system), or (ii) until the time has become long compared to structural response times (milliseconds, depending upon the system). The Split Hopkinson (SHB) is a viable method of measuring the long duration tail of stress pulses generated by radiation or electron-beam deposition induced material blow-off.

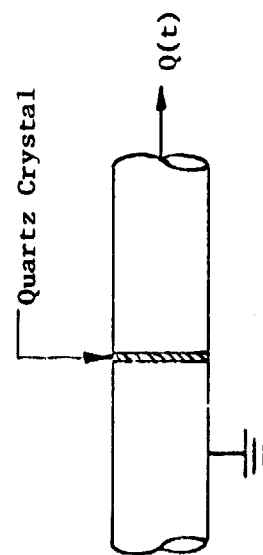
The SHB technique consists of two rod segments, with a piezoelectric crystal cemented between the rod segments (Figure 1). The specimen is located at the end of one rod. A stress wave generated in the specimen, for example by material blow-off, travels down the (front) rod, passes the crystal and into the backup rod. Wavelengths comparable to, or longer than, the rod diameter are propagated essentially unchanged; shorter pulses are strongly attenuated. For a typical 1 cm diameter SHB front rod, stress waves greater than about  $2\mu\text{s}$  long are not significantly attenuated. They compress the thin piezoelectric crystal which releases a charge proportional to the instantaneous stress. This charge  $Q(t)$  is used to charge a capacitor  $C$  to voltage  $V(t)$  according to

$$V(t) = \frac{Q(t)}{C} = \frac{kA\sigma(t)}{C} \quad (1)$$

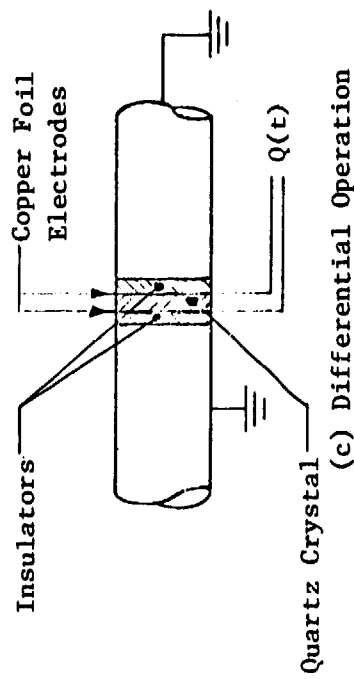
where  $\sigma$  is the instantaneous stress (bars),  $k$  is the crystal piezoelectric coefficient, and  $A$  is the crystal area. With small enough capacitance very large voltages can be produced. Alternately, some crystal materials release more charge than others. Thus, a suitable sensitivity can be obtained by simple choice of crystal material and circuit capacitance. The SHB technique has been used extensively in many areas of experimentation for measuring stress levels from millibars to kilobars.



(a) Split Hopkinson Bar Geometry



(b) Single Crystal



(c) Differential Operation

Figure 1. Split Hopkinson Bar (SHB) and Crystal Configuration

The stress wave is propagated in a rod essentially without distortion whenever the pulse amplitude does not vary significantly in times comparable to the wave transit time across the rod diameter. Thus any slowly varying (compared to 1 to 2  $\mu$ s) pulse tail is not distorted and will be faithfully recorded. Consider a pulse that is approximated by a short duration pulse plus a long duration constant stress tail (Figure 2a). The propagation of the two parts (A & B) down the rod can be treated separately and the results are additive at the sensing crystal location. The narrow main pulse consists of positive step pulse followed by an equal negative step pulse. The step stresses that propagate down the rod to the crystal consist of a finite rise time, followed by oscillatory waves due to radial motion of the rod (Figures 2b & 2c). The net result for the propagated short pulse is as a longer, lower amplitude pulse followed in time by stress oscillations due to the radial motion (Figure 2d). The pulse tail (B of Figure 1), which is assumed to not vary in times long compared to the wave transit across the rod diameter, will propagate unchanged. At the crystal the resultant stress is the simple addition of the constant stress pulse the attenuated main pulse and its oscillations-i.e., the signal will represent the main attenuated pulse with its oscillations superimposed on the constant signal of the pulse tail (Figure 2e). The attenuation of the main pulse in no way affects the signal off-set caused by the pulse tail.

For a step-input pulse on the end of the front rod, the rise time of the propagated wave is a measure of the bar dispersion (Figure 2b). The dispersion results from radial displacement of the rod. When the distance X from the rod front end is greater than about 20 times the rod diameter D, the pulse rise time  $\tau$  scales as

$$\tau \propto \nu^{2/3} (X/D)^{1/3} D/C \quad (2)$$

where  $\nu$  is Poisson's ratio = 1/3 for many materials, and C is the longitudinal wave velocity. Thus, the rise time increases with both length and diameter of the front rod segment and with Poisson's ratio, and decreases with increasing C.

After the wave passes the sensing crystal, it propagates down the second bar segment, reflects at the far end, and returns to the sensor. The useful recording time is terminated at this time, equal to the double transit time in the second bar. For aluminum rods, a 12-inch rod provides about 100  $\mu$ s

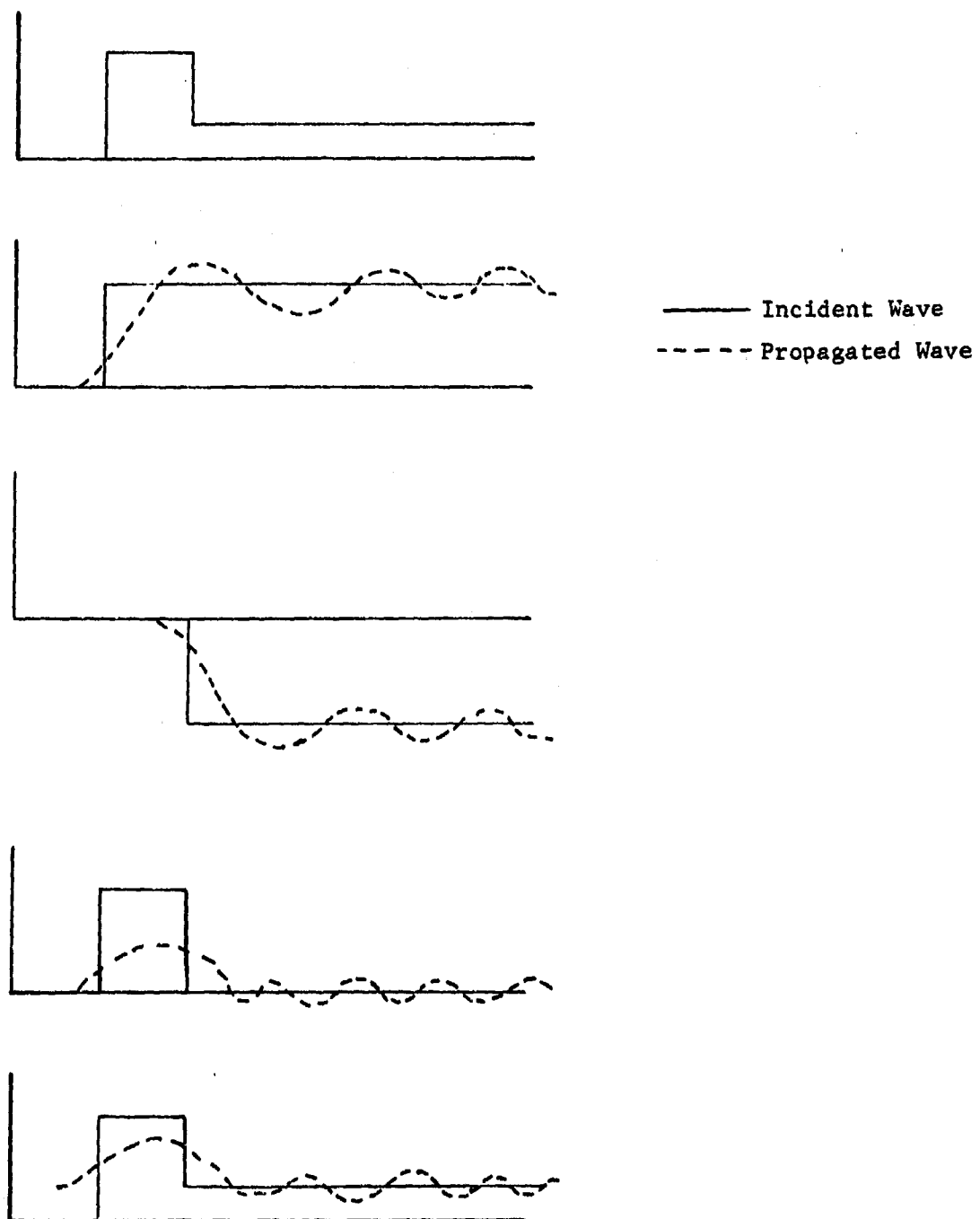


Figure 2. Decomposition of Stress Pulse into Main Pulse plus Pulse Tail--Propagation and attenuation in rods.

recording time. The 10-inch fused silica rods used underground provided a useful recording time of 88  $\mu$ sec.

The potential disadvantages of the SHB are (i) the loss of high frequency stress data, necessitating a conventional one-dimensional stress gauge for time resolution of 1  $\mu$ s or less, and (ii) the circuit must be high impedance (large RC time constant) to assure that the generated charges do not appreciably leak off in times (100 $\mu$ s) of measurement interest. This means that any spurious charges induced on the circuit or cables, due to EMP or Compton secondary electron deposition, must be kept below the charge released by the stress pulse. This is an especially important consideration in electron beam and underground testing. Previous Ktech work with electron beams and in underground tests demonstrated that an SHB operated in a differential mode (Figure 1)(both sides of the crystal isolated from ground and fed into a differential preamplifier) would minimize induce charge problems and avoid noise problems due to ground loops and pipe or cable-shield currents (Reference 1).

Although the SHB was successfully used to record stress histories in both electron-beam and underground tests, a new one-dimensional stress gauge was developed during this program to utilize the thin piezoelectric crystal in the charge mode to overcome disadvantage (i) above thus preserving the high frequency stress data.

## SECTION 2

### PROGRAM OBJECTIVES

This program had three separate objectives:

#### 2.1 SHB Electron-beam Tests

Use the SHB to measure amplitude of the tail of the blow-off stress pulse for heat shield materials (3DQP, TWCP, and Phenolic resin) irradiated with pulsed relativistic electron-beams.

#### 2.2 One-Dimensional Piezoelectric Gauge Development

Develop the charge mode crystal technique used in the SHB for one-dimensional stress measurements with stress resolution of a few bars, time resolution of 20 ns, and recording durations of 10 to 20  $\mu$ sec.

#### 2.3 SHB Diablo Hawk Tests

Design and fabricate two SHB's for fielding in the Diablo Hawk Underground Test Event in support of the DNA, 3DQP Pulse Tail Experiment.

Section 3 discusses the considerations for the electron beam tests and the characteristics of three electron-beam generators used on this program. Section 4 discusses the supporting (one and two-dimensional) stress wave and impulse calculations performed. Section 5 gives the experiment design considerations for both the electron beam and underground test experiments. Results are presented in Section 6 for both the electron beam (SHB and one-dimensional stress gauge) tests, and the underground test.

## SECTION 3

### ELECTRON BEAM MACHINES

#### 3.1 Description

Three different electron beam machines were used in the SHB tests. Three-dimensional quartz phenolic 3DQP and phenolic resin were tested on the GAMBLE I generator at Naval Research Laboratories, in Washington, D.C.. Tape-wrapped carbon phenolic TWCP and 3DQP were tested on the Blackjack 3 generator at Maxwell Laboratories, San Diego, CA. The REHYD generator at Sandia Laboratories Albuquerque, NM was used with 2DQP for the initial tests of the one-dimensional gauge.

These three machines, are quite similar in many respects. They all produce nominally 800 kev mean energy beams, with a duration (FWHM) of 60 ns for GAMBLE I and Blackjack 3, and 90 ns for REHYD. For the purpose of these tests it was desirable to provide a peak dose level of 300 cal/gm, sufficient to cause blow-off of the phenolic resin in the three test materials. This implied a fluence of about 50 cal/cm<sup>2</sup>, an easy requirement for all three machines over the one-half inch diameter of the SHB specimens. However, for the one-dimensional stress gauge tests a much larger exposure area (10 cm diameter → 75 cm<sup>2</sup>) was required. REHYD and Blackjack 3 both have the capability of producing 50 cal/cm<sup>2</sup> over this large area. A brief discussion of the experimental arrangements and beam conditions peculiar to each of the three machines follows.

#### 3.2 GAMBLE I Accelerator

The electrical characteristics of GAMBLE I are shown in Table 1. A schematic drawing of the diode region and experimental set up are shown in Figure 3. The anode consisted of thin 0.001-inch aluminized mylar. A 12-inch long carbon guide cone concentrated the beam onto a one-inch diameter circular aperture. The sample target assembly (SHB) was placed near the end of the guide cone in a 6-inch diameter chamber evacuated to 1 Torr. The fluence was adjusted by varying the machine parameters, primarily the charge voltage. The nominal dose-versus-depth curve is shown in Figure 4 (Ref. 2), normalized to unit fluence. The mean electron energy was about 600 kev, and varied by up to 100 kev from shot-to-shot. The spectrum change is monitored on each shot using voltage and current monitors.

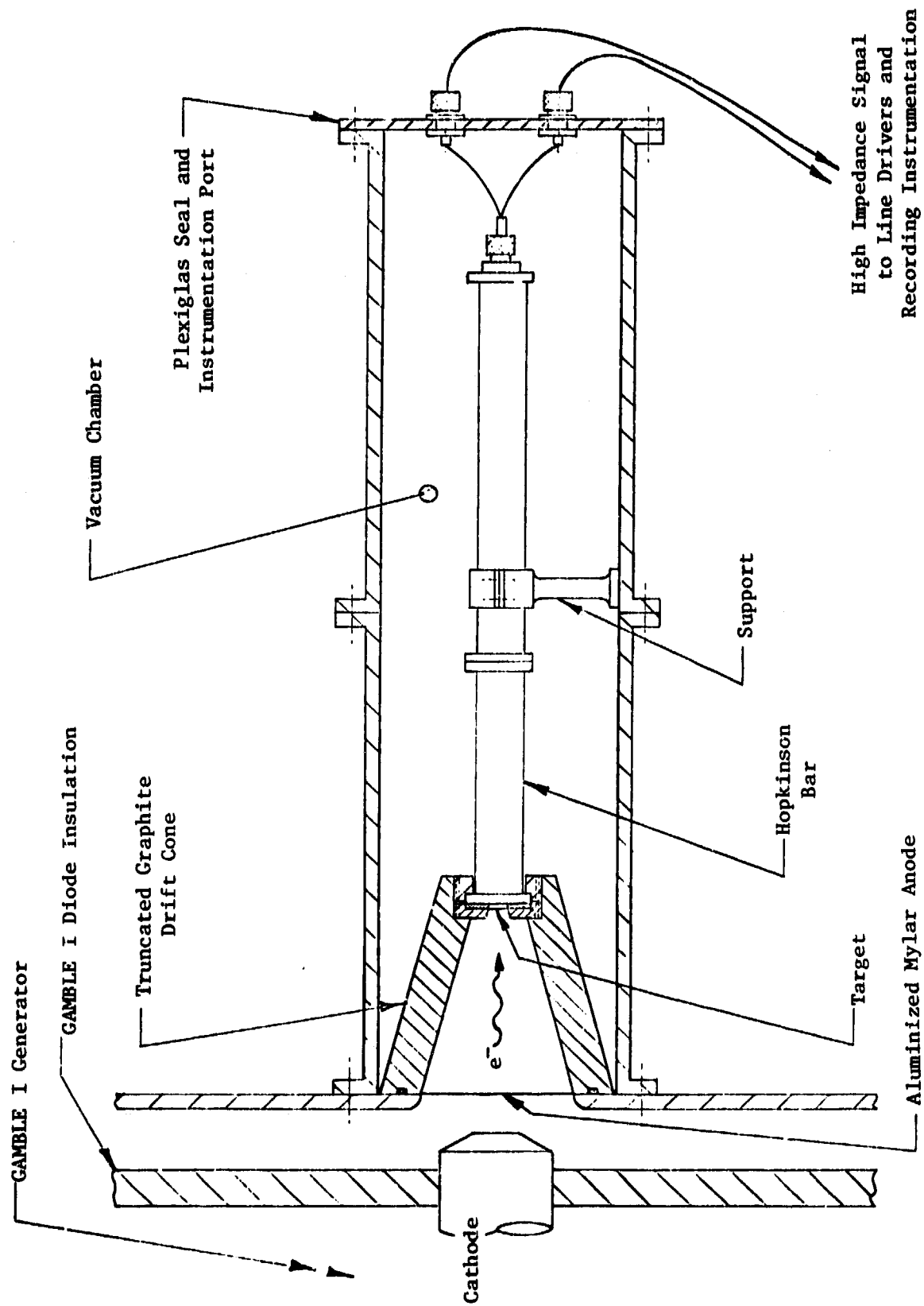


Figure 3. Sketch of diode and experiment geometry for GAMBLE I

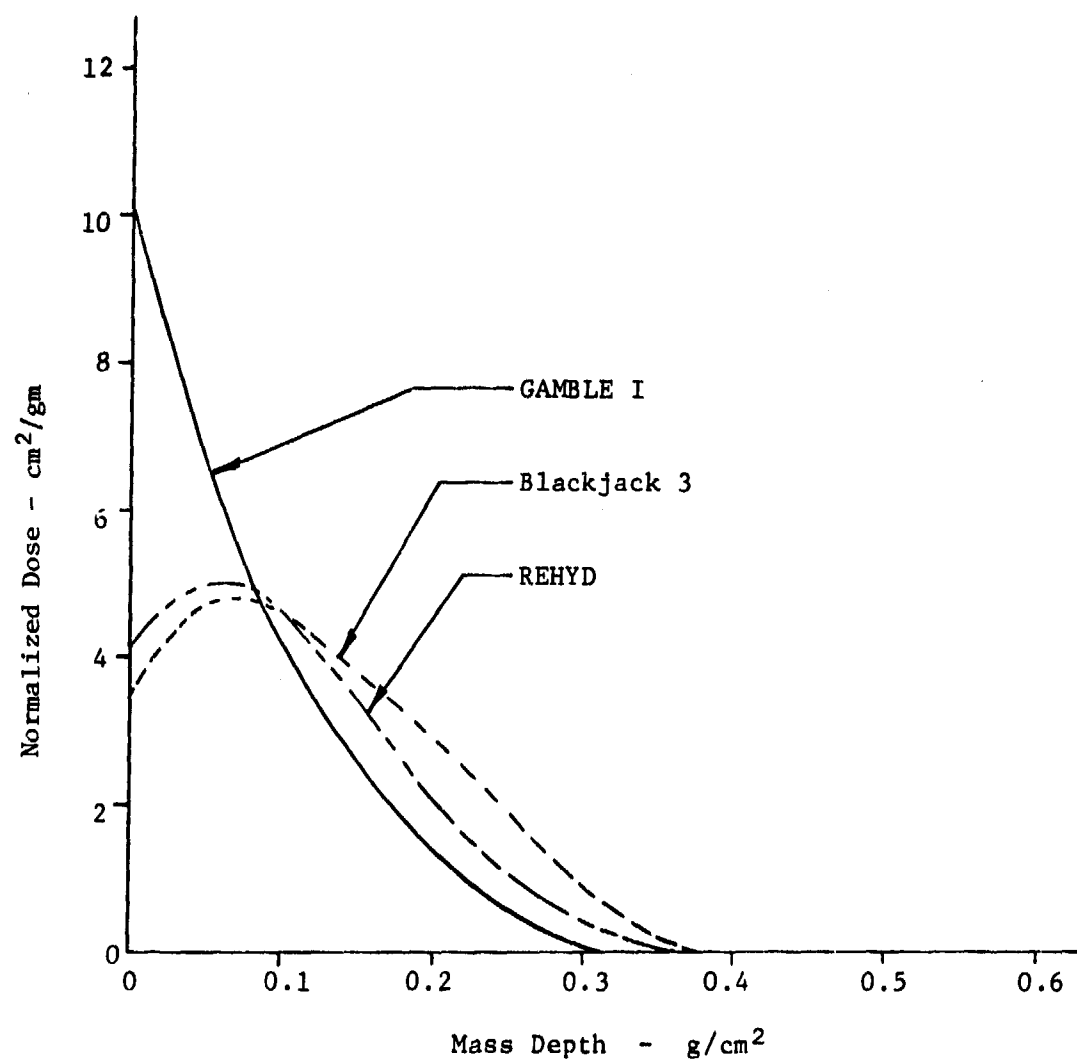


Figure 4. Normalized Depth-Dose Profiles for GAMBLE I, Blackjack 3, and REHYD. Multiply by incident fluence to obtain actual dose-versus-depth

Table 1  
Electrical Characteristics of GAMBLE I, Blackjack 3 and REHYD

	GAMBLE I	BLACKJACK 3	REHYD
Diode Voltage (MV)	0.75	1.0	1.2
Diode Impedance (ohms)	1.5	1	2.5
Current (kA)	250	300	300
Beam Energy (kj)	8	30	25
Pulse Width (FWHM-ns)	60	60	90

### 3.3 REHYD Accelerator

The REHYD diode area is shown in Figure 5. The electrical characteristics of REHYD are included in Table 1 (Ref. 3). The mean electron energy is about 800 kev. The nominal pulse duration (FWHM) is 90 ns, 50 percent longer than the other two machines.

The electron beam was propagated to the target via the axial magnetic field of a large solenoid. This field prevents beam pinching and provides a more repeatable and centered beam onto the target. The target was at 6-inches from the anode, in a chamber evacuated to 0.1 torr.

The REHYD normalized dose-depth curve for the tests conducted on this program is included in Figure 4. The fluence may be varied by changing the Marx charge voltage, and also by the drift chamber pressure and the strength of the external magnetic field. The radial fall-off of the beam fluence is shown in Figure 6.

### 3.4 Blackjack 3 Accelerator

The electrical characteristics are included in Table 1 for comparison with the two other machines. Note the greater total beam energy (34 kjoules) compared to GAMBLE I with the same 60 ns pulse width. Like the REHYD this beam is also propagated to the target using an axial magnetic field; the experimental arrangement is shown schematically in Figure 7. The radial distributions of fluence at 100 and 180 cal/cm<sup>2</sup> are included on Figure 6, and the depth-dose curve is included in Figure 4 (Ref. 4).

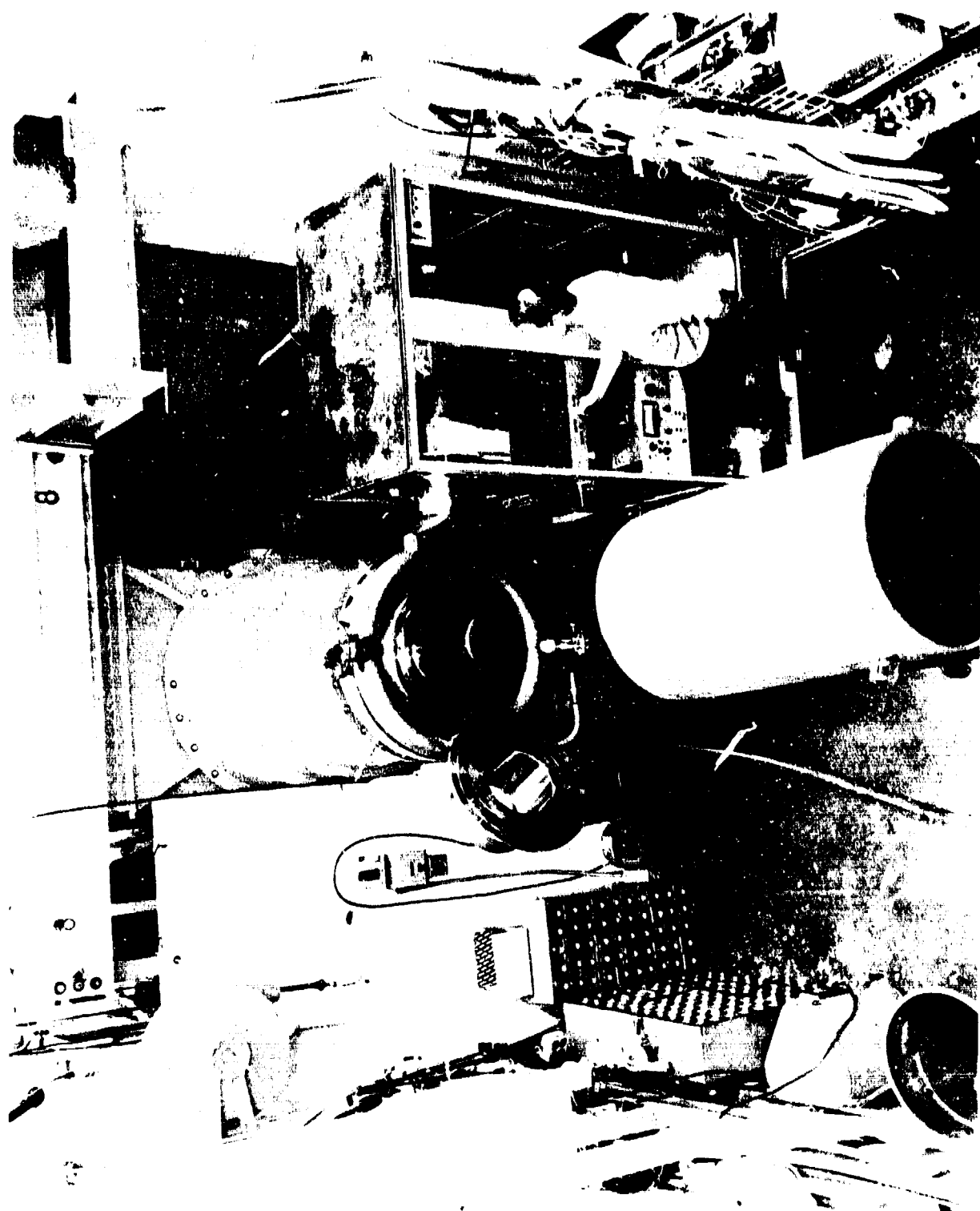


Figure 5. Photograph of REHYD Diode

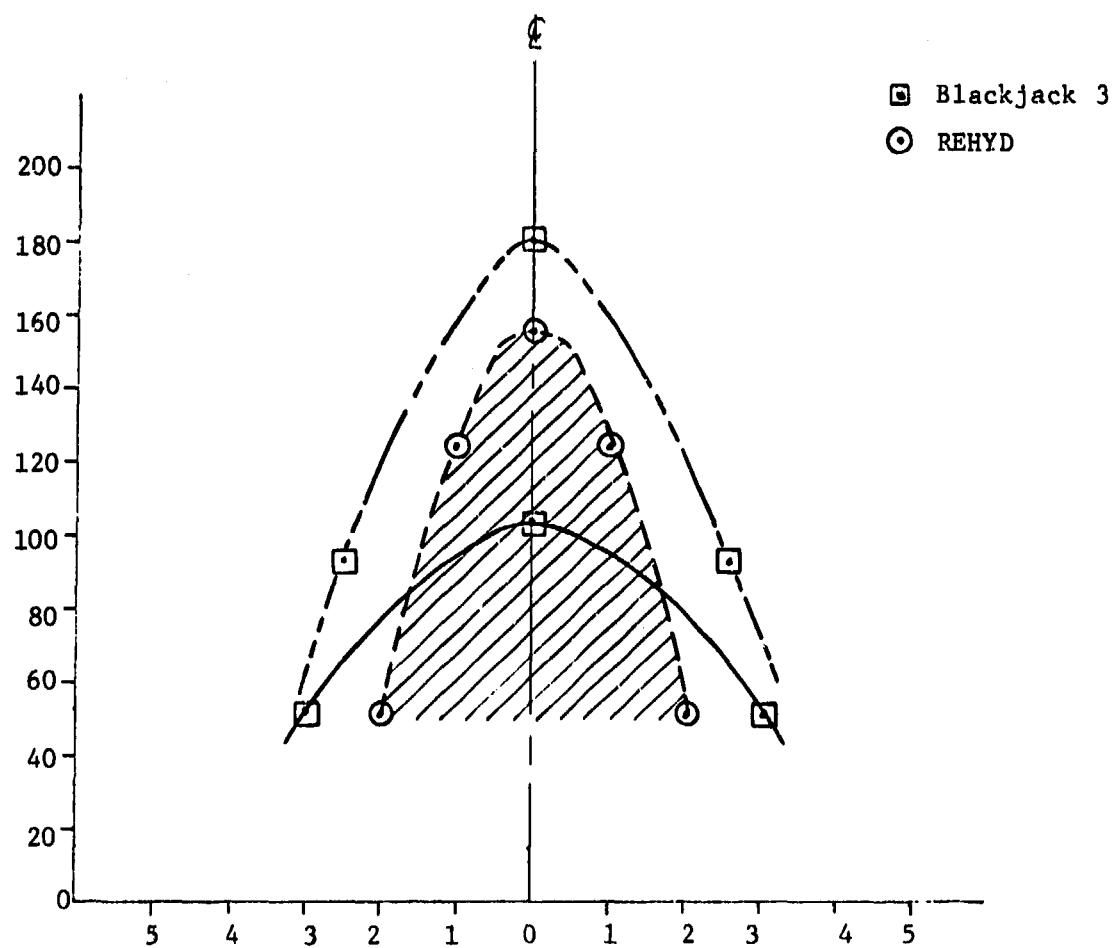


Figure 6. Radial Distribution of Fluence for Blackjack 3 and REHYD.

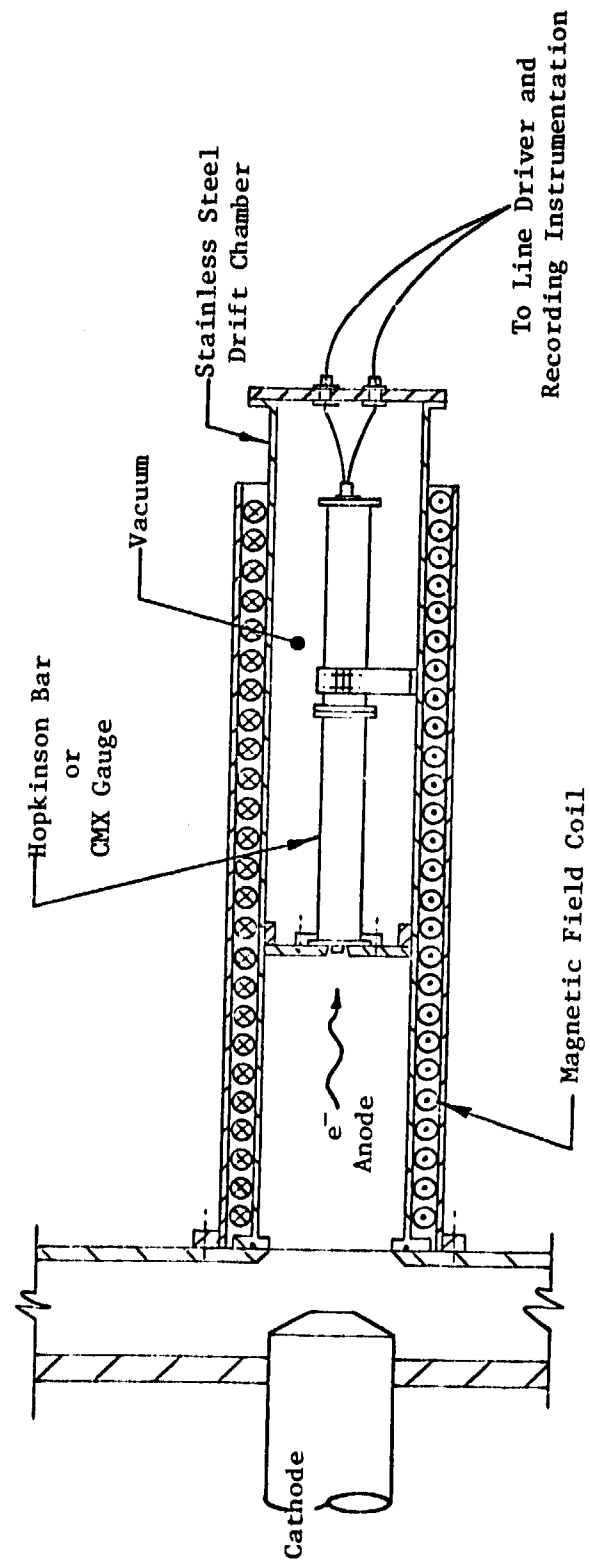


Figure 7. Sketch of Diode and Experiment Geometry for Blackjack 3

### 3.5 Beam Diagnostics

The results of these tests were not meant to be correlated with detailed calculations; rather, they were intended to measure the amplitude of late-time tail of the blow-off stress wave. Therefore, the electron-beam diagnostics were not as comprehensive as would otherwise be the case. The only calorimetric measurements made were the total fluence of each machine. The depth-dose profiles were calculated using the Monte Carlo code ELTRAN (Ref. 1) for each machine using measure voltage and current histories and an electron mean angle of incidence derived from previous Ktech experience with each machine. The calculated depth-dose profiles compared favorably with previous measurements enabling calculation of the blow-off pressure pulse and the total impulse.

## SECTION 4

### CALCULATIONS

Various computer codes were used to calculate the energy deposition profile and the subsequent material response to the blow-off. These calculations were made before the electron-beam tests to determine the electron-beam fluence and mean energy that would simulate the blow-off expected in an underground test. Pre-test calculations were also made for the SHB's to be fielded in an underground test for the purpose of setting the recording oscilloscope sensitivities, and to assure the 3DQP/fused silica rod bond would maintain its integrity during the recording time. The various calculations are described briefly below.

#### 4.1 Deposition Profile

The Monte Carlo computer code ELTRAN (Ref. 5) was used to calculate the deposition profiles for the electron beam tests. This code utilizes the time integrated spectrum deduced from the voltage and current records. The voltage record gives the instantaneous electron energy; the current record give the number of electrons at that energy at that instant of time. Several thousand electron trajectories are followed in ELTRAN to determine the energy deposition versus depth. The principle variable in the code is the mean angle of incidence of the electron, and this parameter is varied until agreement is reached with measured dose-depth profiles. This angle can then be used in conjunction with any spectrum, for calculating the dose profile for any given shot. If the mean electron energy varies, it may be necessary to perform these calculations for each shot using the measured spectrum.

For the purpose of the present program it was not necessary to perform the calculations more than once. The depth-dose profiles shown in Figure 3 were used in all calculations of blow-off impulse and stress generation.

For the underground test SHB design, energy deposition profiles were calculated with the pre-test prediction of the spectrum and fluence using both the GENDEP (Ref. 6) and EDEP (Ref. 7) codes. Calculations were made with several filter thicknesses from zero to 2 mm for the purpose of plotting the peak stress and total impulse variation. The underground test SHB experiment was performed with no filter, as it was determined that the peak stress and impulse would probably not debond the 3DQP specimen from the front of the SHB front rod.

## 4.2 Impulse

Although impulse was not measured separately on any of the experiments in this program, the impulses were calculated for the purpose of comparing the blow-off from the three machines and the underground test, and also for approximate checks on the impulse under the measured SHB main stress pulse. Although the short duration main pulse is rather strongly attenuated in propagation down the rod, the total axial momentum remains constant.

For 3DQP, the prompt (less than 50  $\mu$ s) and total impulses are best obtained using the MBBAY Model (Ref. 8). The prompt impulse is obtained if 350 cal/gm is used for the incipient blow-off specific energy  $E_0$ , and the total impulse is obtained if 200 cal/gm is used for  $E_0$ . The results of the impulse calculations for the three electron beam generators are given in Table 2.

Table 2  
3DQP Impulse Calculations

Electron Beam Generators	Total Impulse* (taps)
GAMBLE I	3.4
Blackjack 3	1.4
REHYD	1.7

\*Based upon MBBAY model for 3DQP with  $E_m = 200$  cal/gm, a fluence of 50 cal/cm<sup>2</sup>, and deposition profiles from Figure 4.

## 4.3 Stress Wave Calculations

4.3.1 One-Dimensional Calculations. The hydrocode PUFF (Ref. 6) was used to calculate the stresses generated by the various electron beam and UGT energy depositions. These calculations were mostly performed by the Air Force Weapons Laboratory (DYV), Kirtland AFB, NM using the PUFF Data (Ref. 6) equations-of-state for the 3DQP and TWCP. These calculations had previously been shown to attenuate the waves quite accurately when compared to laboratory data (Ref. 1). The pulse shapes are not presented in detail in this report as they are not relevant to the conclusions and no attempt was made to correlate them with the

experimental results. However, the peak stress is shown as a function of propagation distance in 3DQP in Figure 8. The calculation was made using the GAMBLE I deposition profile from Figure 3 and a fluence of 50 cal/cm<sup>2</sup>. It is seen that a peak stress of 15 kbars is generated near the front 3DQP surface, and that the peak stress attenuated to about 2 kbar in traversing 0.75-inch of 3DQP. Of course, to conserve momentum, the initial pulse width of 0.2  $\mu$ s FWHM broadens to 3  $\mu$ s over the same distance.

4.3.2 Two-Dimensional Calculations. To calculate the wave propagation down the rod, which length to recording crystal was 12 times the rod diameter, it was necessary to use a two-dimensional code. The hydrodynamic code TOODY (Ref. 9) was used. The PUFF calculations were used to generate the initial stress wave, and to calculate the wave propagated through the specimen (3DQP) and into the front of the rod. The (PUFF) calculated one-dimensional velocity distribution was used for the initial conditions for the rod calculations with TOODY. TOODY was then used to follow the wave and rod motions until the complete wave had passed the sensing crystal location.

This procedure only approximated the actual rod behavior since the 3DQP specimen was not on the rod front for the TOODY calculations. Thus reflected waves due to the specimen/rod acoustic impedance mismatch were ignored in the calculations. For a 3DQP specimen on a fused silica rod, the relative impedances  $Z$  are:

$$Z_{3DQP} = \rho c_o = 0.52 \frac{\text{gm/cm}^2}{\mu\text{s}} \text{ and } Z_{\text{fused silica}} = 1.31 \frac{\text{gm/cm}^2}{\mu\text{s}} \quad (3)$$

Thus the stress wave shocks up in passing from the 3DQP to fused silica: the stress amplification factor is 1.43, so 1 kbar in 3DQP becomes 1.43 kbar in the fused silica rod. The reflected compressive wave, relative amplitude = 0.43, traverses the specimen twice and is further attenuated before arriving as an expansion wave back at the rod front surface. For the specimen thicknesses used (2 cm) this double transit time through the 3DQP was 6.3  $\mu$ sec. These later pulses were considered to be separated sufficiently in time, and sufficiently attenuated that they could be ignored when calculating the propagation of the main pulse down the rod. Note however, that the stress amplification also represents an impulse gain by the same 1.43 factor in the first wave. The subsequent reflected waves would subtract from the first wave

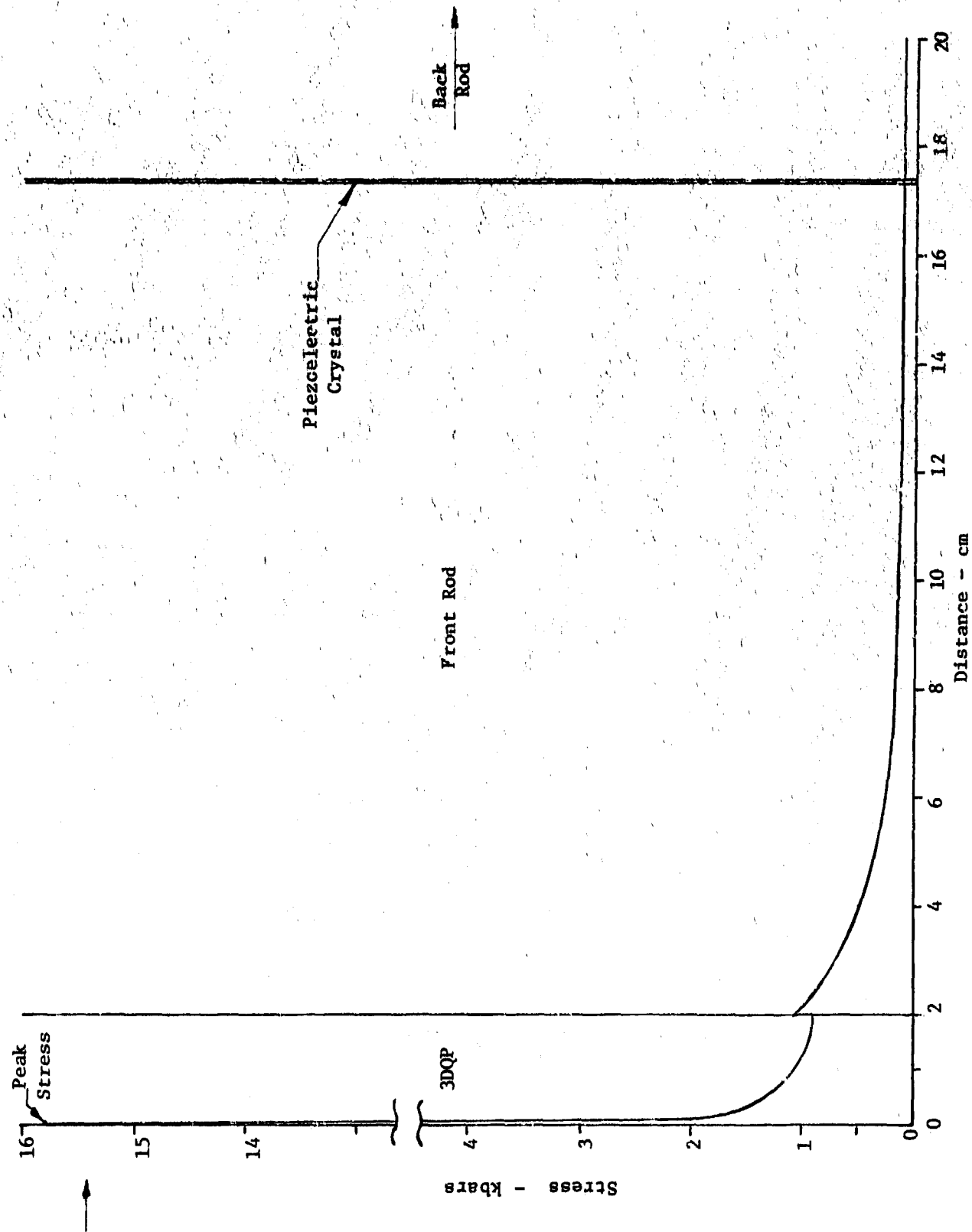


Figure 8. Calculated stress attenuation versus distance for GAMBLE I tests

momentum an amount equal to 0.43 of the 3DQP initial momentum, if the 3DQP remained attached to the rod as was the case in all experiments considered here. Thus the TOODY rod calculations were intended to study the main stress attenuation and spreading down the rod to enable predicting the gauge response for setting the recording oscilloscopes sensitivities.

The rod volume is made up of axial and radial zones. At the front of the rod, the radial zones all have the same initial velocity determined by the PUFF calculations; the velocity varies with axial position. At the axial location of the gauge, the velocity and the stress will vary with radial position. The total gauge stress is the sum of the individual radial zone stresses at any instant of time. Because of the above described simplifications, this summation was not performed and only the stress history of the center radial zone was used.

During the initial calculations, a re-start option was added to the TOODY program enabling the program to be run for some time, stopped, the results examined, and then the calculations continued. This piece-wise operation enabled input changes and corrections to be made early thus greatly conserving computer time. Table 3 lists the various TOODY calculations made. It is seen that calculations were made for various rod materials, lengths and diameters, as well as, with different zone sizes.

Table 3  
TOODY CALCULATIONS

<u>FILTER</u> (cm Graphite)	<u>ZONE SIZE</u> (cm)	<u>RUNNING TIME</u> ( $\mu$ s)	<u>ROD</u> <u>CONFIGURATION</u> (dia-cm/material)	<u>COMMENTS</u>
none	0.1 axial 0.05 radial	40	1.27/SiO <sub>2</sub>	No deposition in SiO <sub>2</sub>
none	0.1 axial 0.05 radial	40	1.27/SiO <sub>2</sub>	with deposition in SiO <sub>2</sub>
0.025	0.1 axial 0.06 radial	10	1.27/SiO <sub>2</sub>	with deposition in SiO <sub>2</sub>
0.025	0.1 axial 0.1 radial	10	1.27/SiO <sub>2</sub>	with deposition in SiO <sub>2</sub>
0.025	0.1 axial 0.05 radial	40	1.27/SiO <sub>2</sub>	with deposition in SiO <sub>2</sub>

## SECTION 5

### EXPERIMENT DESIGN CONSIDERATIONS

#### 5.1 Split Hopkinson (SHB) Design

The SHB was designed primarily for underground test measurement of stress pulse tail. The SHB used for the electron beam tests was the same except for different rod materials and lengths. There are three major areas of concern in the design of a Split Hopkinson Bar to be fielded in an underground test. These are the design of the bar itself, the cassette design, and the electronics used to process the signal generated in the sensitive element. These three areas are discussed separately.

5.1.1 Bar Design. The design of the SHB for use in a UGT environment requires not only the usual materials and sizing considerations, but also a consideration of the radiation effects on the bar material and the piezoelectric element. This includes X-ray effects, which can be well predicted, and the gamma and neutron effects, which can only be qualitatively estimated. The X-ray deposition profiles were calculated using the computer program GENDEP (Ref. 6) and the resulting stress wave propagation was predicted using the hydrodynamic programs PUFF (Ref. 6) and TOODY (Ref. 9).

The results of the deposition calculations for the underground test spectrum showed that sufficient fluence would be transmitted through a 3DQP test specimen to produce significant stress generation in a metallic front rod. Based on these results, it was decided to use the thickest practical 3DQP specimen, 2 cm, backed by a fused silica front rod. Because of its low Gruneisen coefficient ( $\Gamma=0.035$ ) the calculated 18 cal/gm deposited in the front of the fused silica rod would generate only 60 bars stress. Further, the deposition profile in the fused silica was steep enough that this small pulse would last only about 1  $\mu$ sec. This silica pulse would manifest itself as an early rise on the leading edge of the QP pulse, but not affect the measurement of the pulse tail. Finally, the front rod length was sufficient to shield the sensing crystal from X-radiation.

The sizing of the bar itself was based on a number of considerations. The front rod had to be long enough to provide sufficient delay to permit the electronics to stabilize from the gamma and neutron pulses. The length of the

front bar is generally based on the requirement that nonuniformity of loading not propagate to the location of the sensitive element (a length greater than 20 diameters assures this). Since the X-ray (and electron) loading was very uniform, a length of 10 diameters assured a one-dimensional stress field at the crystal. It was desired that the backup rod be of sufficient length to permit 50 to 100  $\mu$ s of recording time.

The selection of the diameter of the bar is a trade-off between bar frequency response (which varies inversely with diameter) and the output of the sensitive element (which varies directly with crystal area). An additional consideration is the structural integrity of the bar, which prohibits the use of very small diameter bonded bars. A rod diameter of 1.27 cm was chosen; the wave transit across a rod this diameter is 2.1  $\mu$ s, which is the lower limit on the time resolution for these rods. Stress variations in less than 2  $\mu$ s would attenuate severely while those stress variations occurring over longer times would not attenuate significantly. The sensitive element selected was an X-cut quartz disc 0.020 inches thick, giving a crystal response time (one wave transit across the crystal) of 0.08  $\mu$ sec. Quartz is well characterized in both loading and unloading, its output is linear over the stress amplitudes of interest here, and its responses to gamma and neutron radiation are known. In addition quartz provides a good mechanical impedance match to the fused silica rods, and also to aluminum rods, thus minimizing the quartz disk equilibration time.

Based on the consideration given above, the bar shown in Figure 9 was designed. For the Diablo Hawk event, the test specimen was a disc 2.0 cm thick of 3DQP with the same 1.27 cm diameter as the rod. The front rod was 15.24 cm of fused silica, 1.27 cm in diameter ( $L/D = 12$ ). The sensitive element used was 0.05 cm X-cut quartz, and the backup rod was 25.4 cm of fused silica.

Thin copper foils were bonded between each rod section and the crystal to serve as electrodes. All bonds were made with EPON 828\* epoxy with HYSOL 3490 hardener<sup>†</sup>. All bonded surfaces were first ground flat prior to assembly in a special jig which insured proper alignment of the four section of the bar: specimen, front rod, crystal, back rod. The two electrodes were connected to

---

\* Trade name of Shell Chemical Company, One Shell Plaza, Houston, TX.

<sup>†</sup> Hysol Division of The Dexter Corporation, Los Angeles, CA.



the center conductors of two coaxial cables, which were twisted and brought to the rear of the SHB cassette. The coaxial cable shields were grounded to the cassette and the two center leads, isolated from ground, were fed into separate signal conditioning electronics.

The piezoelectric sensitivity of the X-cut quartz crystal, operated in the charge mode is 2.704 picocoulombs/Newton. The charge released is directly proportional to the average stress in the crystal. This results in a circuit voltage output  $V$  (volts) inversely proportional to the circuit shunt capacitance  $C$  (Equation 1):

$$V = 27 \frac{\sigma}{C} \quad (4)$$

where the stress  $\sigma$  is in bars, and the total circuit capacitance  $C$  is given in picofarads. The total circuit capacitance typically consisted of the crystal capacitance (60 pF), the coaxial cable capacitance and the input capacitance of the electronics. For example, with 84 feet of cable (at 28.5 pF/foot) between the crystal and recording oscilloscope (input capacitance 48 pF each channel),  $C=1200$  pF, and the overall circuit output is 22 volts/kbar. Obviously this sensitivity is easily changed by suitable choice of  $C$ .

5.1.2 Collimator. For either electron beam or UGT tests it is necessary to collimate the irradiation source to match the 1.27 cm specimen diameter. For electron beam tests a simple graphite absorber thicker than the electron range and with a 1.2 cm diameter hole was used. For underground testing an annular absorber was used to protect the front end of the cassette, as shown in Figure 10. The absorber consisted of successive layers of ATJ graphite, fused silica, aluminum, titanium, carbon foam, tantalum, and a thick polyurethane foam shock pad which served to shock isolate the absorber from the end of the cassette. Each layer thickness was selected to limit the energy deposition in the next layer to less than the melt or spall levels.

Deposition in the collimator will cause stresses in each material. In the electron beam tests simply spacing the collimator away from the SHB cassette isolated these stress from the bar. In Diablo Hawk, the collimator was glued onto the end of the cassette. It is not known how much collimator stress would be transmitted through the "O" ring rod supports, but it was known (e.g., by simply tapping on the cassette) that the "O" ring isolation is not perfect and a significant pulse can be obtained this way. This was one argument for

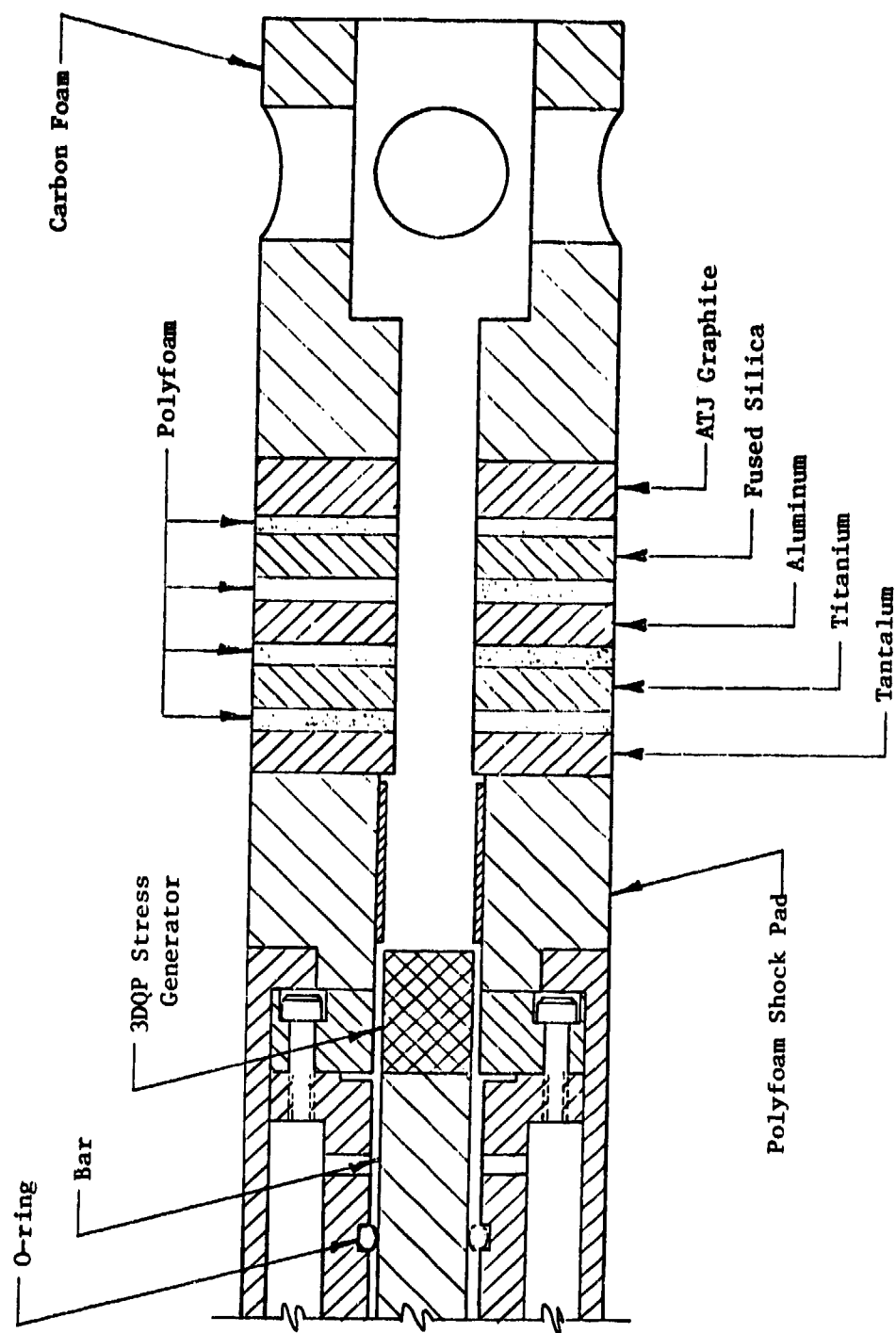


Figure 10. SHB Collimator for underground test application

using, in underground tests, a background gauge for which there was no hole in the absorber/collimator and hence no specimen generated stress.

5.1.3 Cassette Design. The primary requirements for the cassette design were to provide shock isolation and structural support for the bar, and electrical connection to the crystal faces. The cassette provided lateral bending support without affecting axial wave propagation.

The Ktech cassette design is shown in Figure 9. The bar is supported in the three-piece rod holder with "O" rings which provide the required lateral constraint without producing significant axial constraint. The bar and holder are assembled together with the holder serving as the bar alignment jig. The bar holder is then mounted in the outer cover which provides mounting support for the collimator assembly, and a threaded bulkhead mounting stud. This cassette was used extensively for electron beam and magnetic flyer system-check testing and proved highly reliable and provided a great deal of flexibility in bar component installation and replacement.

Split Hopkinson Bars were manufactured with aluminum, beryllium, fused silica, and plexiglas rod materials providing a variety of sound speeds and Poisson ratios. All rods were 0.5-inch in diameter, providing a time resolution of 1 to 4  $\mu$ s depending upon the material. The front rods were 4 and 6 inches long; the rear rods either 10 or 12 inches long, providing recording times to 192  $\mu$ s (plexiglas rear rods).

Two piezoelectric crystals, X-cut quartz and lithium niobate ( $\text{LiNbO}_3$ ), were used to record the stress waves transmitted down the front rod. The relative sensitivities are given in Table 4, column 2.

Table 4  
GAUGE SENSITIVITY (See Eq. [1])

Crystal	Crystal Sensitivity, k (coulombs/cm <sup>2</sup> )/bar
X-cut quartz	$2.704 \times 10^{-11}$
$\text{LiNbO}_3$	$7.3 \times 10^{-11}$

It is seen that  $\text{LiNbO}_3$  crystals produce three times more charge, and hence signal than does quartz. Both crystal materials were 0.020 inch thick, thin enough so as to not be too fragile and yet not limit the resolution time of the SHB. Both crystals were used in the electron beam tests; only quartz was used in the Diablo Hawk SHB's.

5.1.4 Signal Conditioning Electronics. The piezoelectric gauge for the SHB is thin enough to be nearly uniformly stressed, and is used in the charge mode where the charge generated is directly proportional to the average stress in the crystal. The circuit impedance must be high so that the RC decay time is long compared to the desired recording time (100  $\mu\text{s}$ ). This also means that radiation induced charge in the circuit does not bleed-off, and this charge constitutes a potential difficulty in applying this type of circuit with electron beam or in UGT's. To mitigate the potential induced charge problem, Ktech designed an electronic crow-bar circuit that shunts the coaxial cables until some time after the noise source, has died out, and opens up at a pre-determined time so the circuit becomes high impedance shortly before the stress wave arrives at the crystal position. Then any charge induced onto the cables before they become high impedances is bled-off.

This crow-bar circuit was added to the front end of the Ktech Safety Line Driver (KSLD), which is a solid state operational amplifier (unity gain) with  $10^{11}$  ohm input impedance and a charge follower circuit for driving line cables to the recording instrumentation. Two such KSLD's with a single crow-bar circuit are required for each differentially operated SHB. For UGT application these line drivers are necessary for driving the long cables; for electron beam testing they are necessary to reduce the cable length (crystal to line drivers) to either increase the circuit sensitivity or to increase cable ringing to a high enough frequency to be undetectable.

The simplified schematic for the KSLD and crow-bar is shown in Figure 11. It was estimated that the electronics would be sufficiently shielded in an underground-test alcove to prevent any direct transient or permanent radiation damage to the components, an assumption which proved correct by the successful results and by postshot examinations.

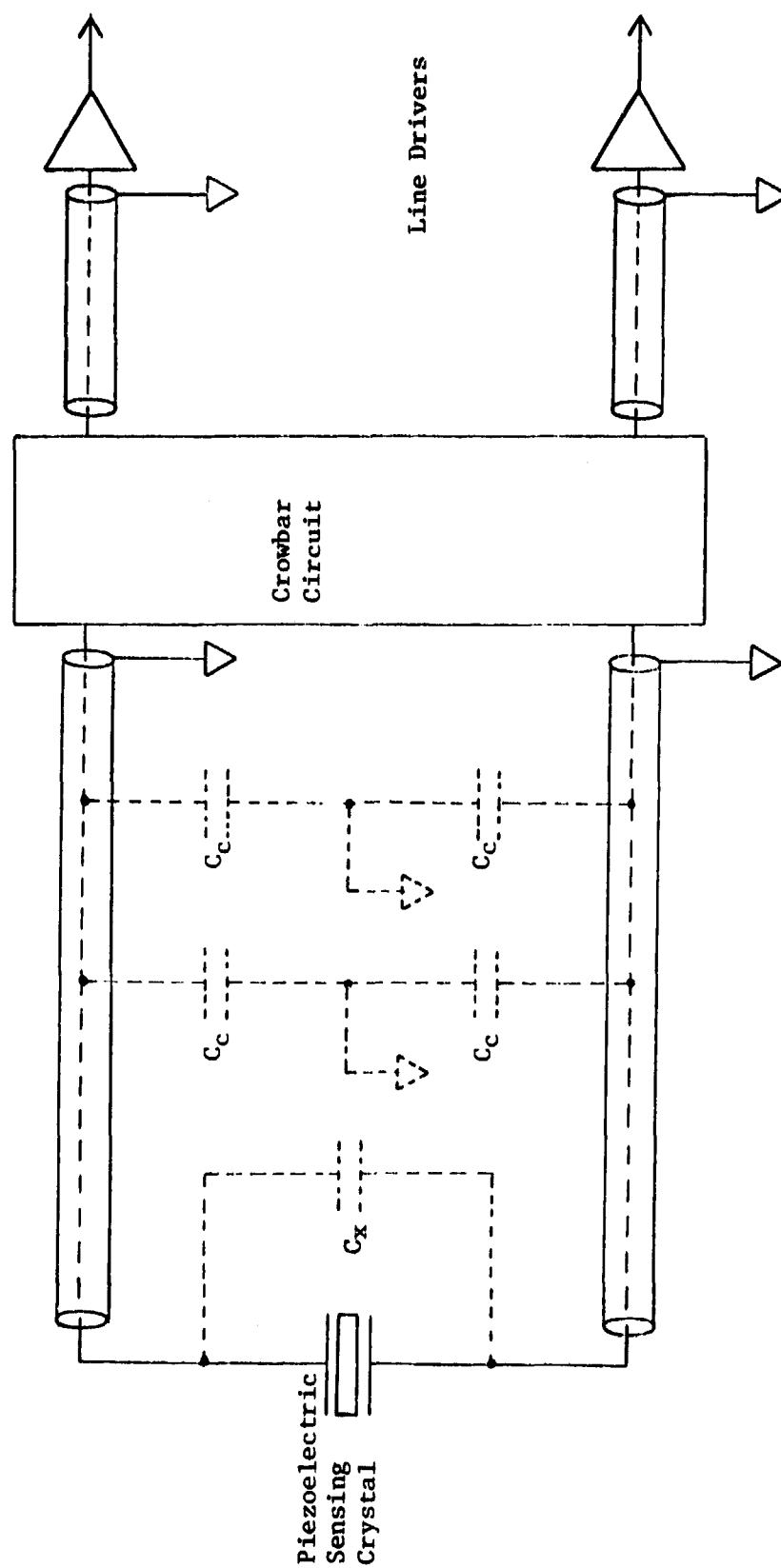


Figure 11. Simplified Schematic for SHB and signal conditioning electronics.

It is of course essential that the line drivers not alter the pulse wave form. To determine that this was the case, extensive laboratory testing was performed with the SHB mounted in the cassette and impacted with a ball-drop. The resulting signals were recorded on oscilloscopes both with and without using the line driver. In addition, because the ball drop gave rather long pulses (50  $\mu$ s), the line drivers were tested for short duration electrical pulse inputs simulating the SHB output from a short stress pulse.

The principal results from these tests show that both the high and low frequency pulses are very faithfully passed by the line driver. Equally important, there is no baseline shift or drift caused by these line drivers.

5.1.5 SHB Calibration. The absolute calibration of the SHB is very well known since it is determined by the known piezoelectric coefficient for the sensing crystal (See Table 4). However, a determination of the overall SHB sensitivity is easily made by using ball drop tests as follows. The above piezoelectric coefficient and the known total circuit capacitance give a direct proportionality constant between stress  $\sigma$  and circuit voltage  $V$ . The stress history  $\sigma(t)$ , obtained from the voltage record, is integrated to determine the total momentum  $I_0$  delivered to the rods. This momentum is also obtained from the initial ball height  $h_i$ , rebound height  $h_r$ , ball mass  $m$ , and crystal area  $A_c$ :

$$I_0 = \int_0^{\infty} \sigma dt = \frac{m_0}{A_c} \sqrt{2g(h_i + h_r)} \quad (5)$$

The two impulse values agreed to better than 1%, thus verifying the SHB stress sensitivity.

## 5.2 One-Dimensional Piezoelectric Gauge-CMX Gauge

The output for conventional current-mode piezoelectric (quartz,  $\text{LiNbO}_3$ ) gauges is proportional to the difference in stress between the two gauge surfaces. Thus, the useful recording time for this type of a gauge is one wave transit time across the crystal. This is typically 1 or 2  $\mu$ sec. Longer recording times are necessary to map out complete stress histories in many cases; to study the low amplitude tail of a stress wave great sensitivity is also required. Thin in-material piezoresistive stress gauges (mananin foil and carbon film) can be used for long recording times, but they lack the sensitivity for measuring in the few tens of bars stress regime.

The successful application by Ktech of thin piezoelectric crystals in the charge mode for SHB material (one-dimensional stress) measurements in both electron-beam and UGT environments meant that this technique could be considered for other gauge geometries. Specifically, as part of this program, Ktech has successfully developed and applied the charge mode crystal sensor in a one-dimensional strain geometry. This gauging technique has the advantages of great sensitivity ( $<1$  bar) for long times ( $>10$   $\mu$ s, limited only by the stressed area). The charge mode crystal, termed CMX gauge when used in a one-dimensional strain geometry, is nominally 1 cm diameter by 0.005-inches thick, and is mounted as shown in Figure 12. The resolution time for a 0.005-inch thick quartz crystal is 20 ns, comparable to in-material piezoresistive gauges. This may be compared with the microsecond resolution for a one-half inch diameter SHB. The stress sensitivity is just the same as when the crystal is used in a SHB, and depends upon the crystal piezoelectric sensitivity and the circuit capacitance. Thus, the CMX gauge has both excellent time and stress resolution. The recording time is determined by the specimen diameter only, or in the case of the electron-beam tests by the radial size of the irradiated area. In UGT tests this time can be made very large. If the gauge is imbedded in a material with sound speed 0.3 cm/ $\mu$ s, a 10  $\mu$ s one-dimensional recording time requires a specimen only 6 cm in diameter.

Figure 13 shows a CMX-gauged target assembly made up with the crystal between a quartz phenolic target and a Plexiglas backplate. The crystal is the small visible circle with two leads. In this example, the Plexiglas backing was used so a laser interferometer could monitor the rear surface motion of the crystal directly. This measurement simultaneously with the gauge measurement provided direct independent confirmation of the CMX gauge calibration, and demonstrated the gauge ability to accurately follow the stress pulse for a longer time than the interferometer, and with greater sensitivity.

This new CMX gauge concept was tested in electron-beam exposures using the Maxwell Blackjack 3 and Sandia REHYD large area beam generators. The results are discussed in Section 6.2.

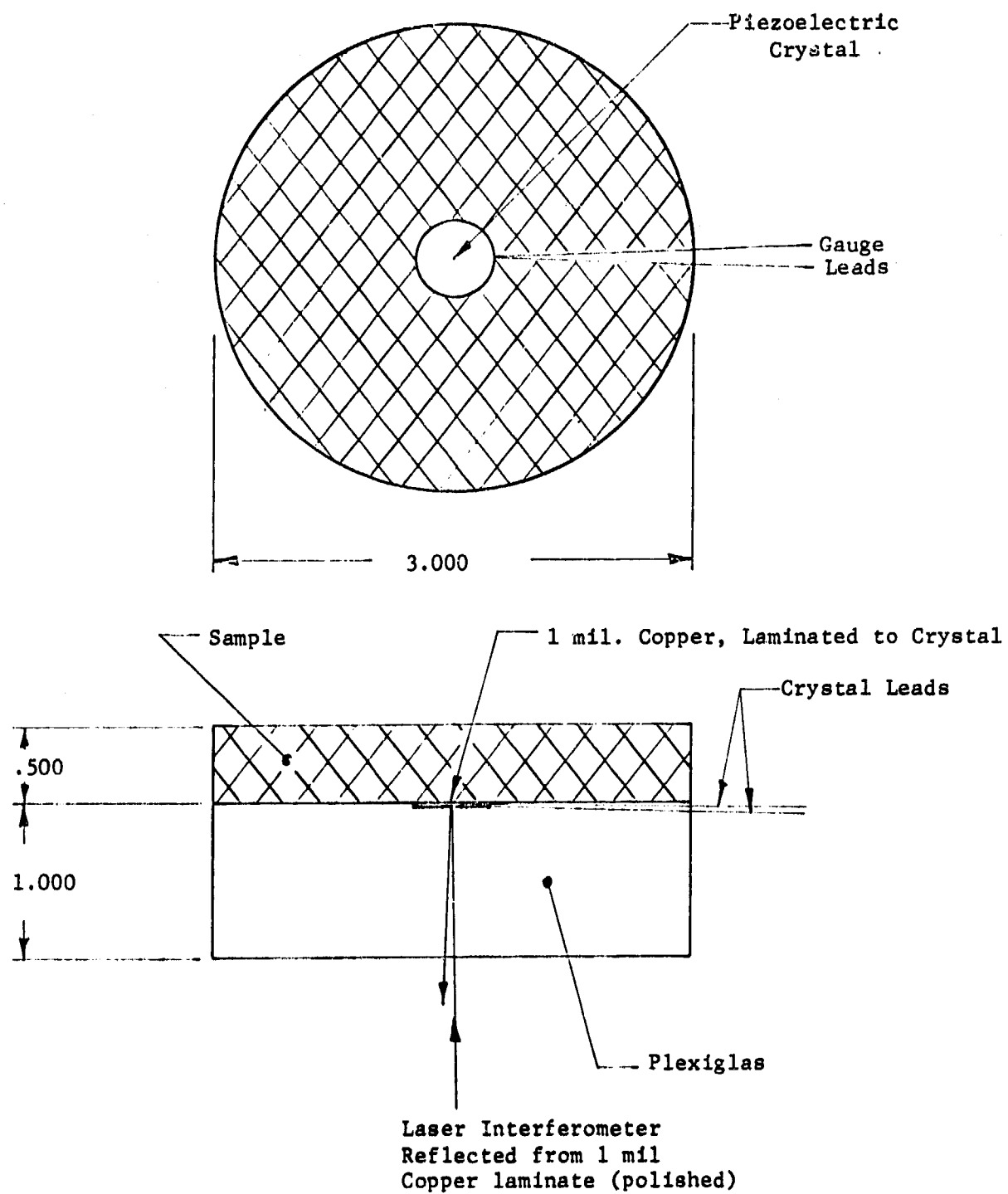


Figure 12. Sketch of One-dimensional charge mode crystal gauge-CMX.



Figure 13. Photograph of CMX gauge assembly with a quartz phenolic target backed by Plexiglas used in Shot No. 2122.

## SECTION 6

### RESULTS

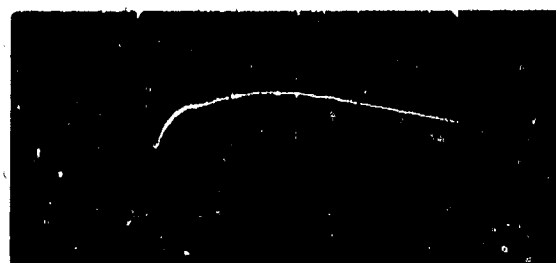
#### 6.1 Electron-Beam Results with SHB

The initial electronic system response and noise checks were made using a Febetron 705 located at Sandia Laboratories, Albuquerque. This 2-MeV machine will produce 20 cal/g. Various grounding and shielding schemes were tried until acceptable noise levels were obtained. No actual stress measurements were made when using this machine.

The GAMBLE I electron beam accelerator at the Naval Research Laboratory, Washington, D. C., was used for the first stress test series on 3DQP and phenolic resin. The beam fluence was adjusted to provide a nominal 50 cal/cm<sup>2</sup> onto the specimen. This condition provided a blow-off depth, and energy deposition to this depth, approximating that expected in underground tests. The deposition profile for this beam is shown in Figure 4. The 3DQP blow-off impulse was estimated (by MBBAY calculation with melt energy 150 cal/g) to be 3.4 ktaps.

A total of 25 exposure tests of the SHB were made using the GAMBLE I generator in three and a half days of testing. Various combinations of sample and rod materials were used with the two piezoelectric crystals. Not all of the shots will be presented in this report since many repeated and confirmed other shots; only the significant results will be presented, along with representative records obtained with the SHB.

6.1.1 Noise Level. With the SHB in place near the end of the guide cone, the first shots were made with a carbon absorber in front of but spaced away from the sample to absorb all of the electron beam. In this manner no stress was introduced into the SHB and so only the electrical noise levels were determined. Figure 14 shows a typical result (Shot No. 6040); the noise level was 16 mV, which corresponds to a 0.24-bar stress level for the LiNbO<sub>3</sub> crystal used. This same voltage would correspond to a 1-bar stress noise for a quartz crystal. This noise level was considered very good, since an actual stress of only 10 bars would then result in signal-to-noise ratio of 25:1 for LiNbO<sub>3</sub> and 10:1 for quartz. This noise level persisted for about 50  $\mu$ sec.



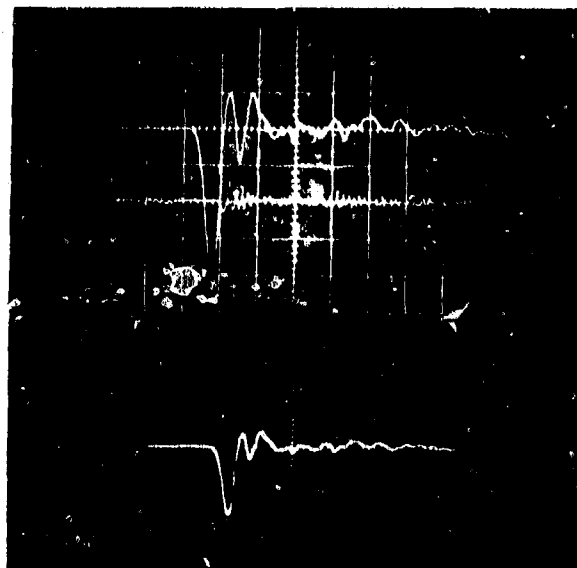
10 mv/division  
75 bars/division

Time → 5  $\mu$ s/division

Figure 14. SHB noise test. GAMBLE I Shot No. 6040.  
LiNbO<sub>3</sub> crystal in plexiglas rod. Sensitivity  
is 14.9 bars/volt.

6.1.2 3DQP Results. Figure 15 (Shot 6042) shows a typical result obtained using GAMBLE I. The short main stress level was 340 bars from the 3DQP blow-off. This is considerably reduced in amplitude from the calculated initial 3DQP Gruneisen stress ( $\approx 15$  kbar, not measured), as expected because of attenuation in the 0.75-inch 3DQP (to about 2 kbar), followed by the subsequent attenuation suffered in propagating down the front rod (refer to Figure 8). This rod attenuation for high frequency pulses is just that discussed earlier. Note that the main pulse is also widened to about 7  $\mu$ s, so that the total momentum is conserved.

The most important results of shots such as No. 6042 are obtained by examining the record following the main pulse. Any late time stress pulse would manifest itself by a displacement of the oscilloscope trace from the zero stress level (which is the trace location seen before the main pulse). It is seen that for Shot No. 6042, within 20  $\mu$ s after the main stress wave there is no discernable trace offset--i.e., no stress after this time, which with a resolution of 0.1 division, means that any such late stress is less than 8 bars! The oscillating nature of the scope trace is characteristic of short stress pulses transmitted down rods, and is very well calculated by computer programs such as TOODY, provided the input stress history is well known. The fact that the oscillations (which are less than 25 bars after 20  $\mu$ s) are about a zero stress level is the indication that the late time stress is as low as stated. This result was repeated on several tests on both GAMBLE I and Black-jack 3 generators.



2.3 Volts/div.  
85 bars/div.  
10  $\mu$ s/div.

8.0 Volts/div.  
296 bars/div.  
50  $\mu$ s/div.

4.0 Volts/div.  
148 bars/div.  
10  $\mu$ s/div.

Time →

Figure 15. SHB result for 3DQP. GAMBLE I Shot No. 6042. Quartz crystal in aluminum rod. Sensitivity is 37 bars/volt. Area under main pulse gives 1360 taps areal impulse.

6.1.3 TWCP Results. Figure 16 shows a typical example obtained on Tape Wrapped Carbon Phenolic using the Blackjack 3 electron beam generator. As was the case with 3DQP, there is again no observable pulse tail stress. The stress recovers to zero within 20  $\mu$ s, or earlier. The radial ringing of the rod causes oscillation in the signal about zero stress with a resolution of less than or equal to  $\pm 0.1$  division, corresponding to 7 bars. The lower trace, at a slower sweep speed, also shows two reflected pulses: the first is the main pulse arriving at the crystal after reflecting from the far end of the backup rod. The next pulse arrives at the crystal after a shorter time interval and represents the subsequent transmission to the front of the rod, reflection and subsequent arrival again at the crystal. Reflection at a free end reverses the polarity of the pulse.

6.1.4 Phenolic Resin. At the start of this program, it was not known whether a pulse tail stress existed or not for 3DQP and TWCP. If it did exist, then it would be important to also test phenolic resin alone to ascertain the cause of the late time stress. Thus phenolic resin was included in the test program. Phenolic resin was bonded to the end of a SHB using plexiglas rods for a good impedance match. Exposures were made during the GAMBLE I tests. The results are essentially the same as for the two composites. As shown in Figure 17, within 10  $\mu$ s of the main stress peak, the stress falls to zero with a resolution of  $\pm 2$  bars.

Thus we find that all three materials show no observable pulse tail greater than about 5 to 10 bars after only 10 to 20  $\mu$ sec. These experiments show the very important result that the stress quickly falls below levels of system interest. The late time stress level is of interest, however, because it can add significant impulse. Thus 1 bar acting for a millisecond would add one kilotap to the total late time impulse. This would mean that total impulse gauge measurements would not be appropriate for understanding or correlating with either material or structural responses.

The SHB can easily be used to record stresses of less than 1 bar. However, when such a low amplitude stress is preceded by a much larger pulse, the resultant radial rod oscillations will be of substantial amplitude that they make greater resolution of the pulse tail impossible. Using the SHB, the resolution of the pulse tail measurement cannot be much better than the results

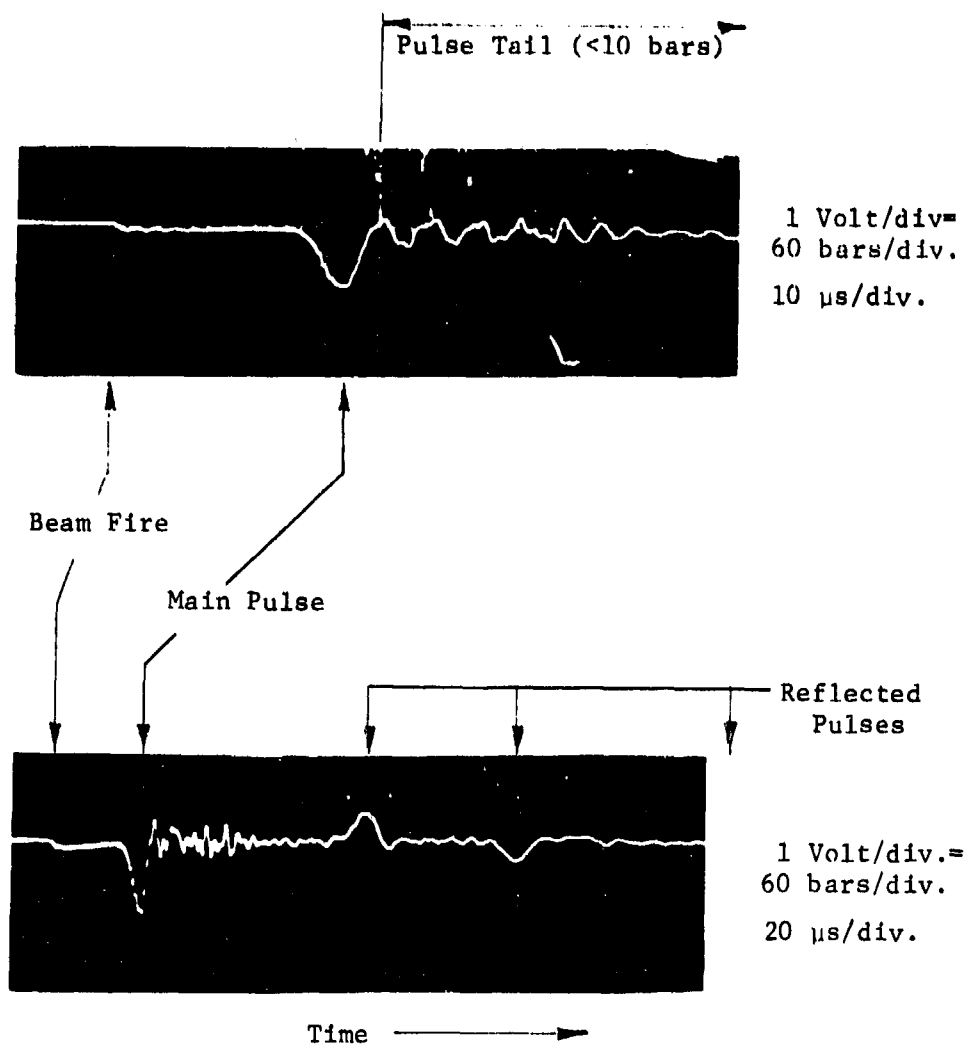
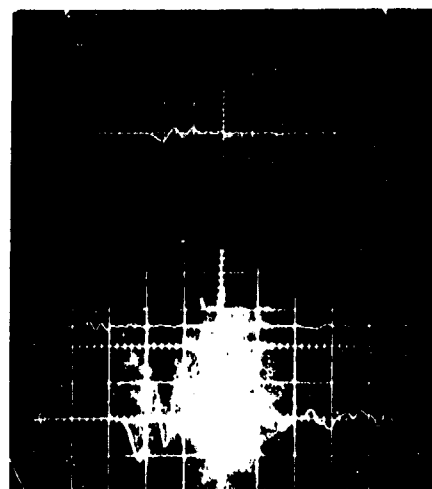


Figure 16. SHB result for TWCP. Blackjack 3 Shot No. 2164. Quartz gauge in Plexiglas rod (4 inch front rod, 8 inch back rod).



8 Volts/div.  
120 bars/div.  
10  $\mu$ s/div.

20 Volts/div.  
300 bars/div.  
20  $\mu$ s/div.

1 Volt/div.  
15 bars/div.  
10  $\mu$ s/div.

Figure 17. SHB result for Phenolic Resin. GAMBLE I Shot No. 6046. Lithium Niobate gauge in Plexiglas rod. 0.020 inch ATJ graphite filter and tamper in front of specimen.

given in this program. In order to obtain better resolution on the pulse tail, it is necessary to eliminate the radial oscillations of the rod--one way is to utilize a one-dimensional strain geometry. This was done using the CMX gauge and the results are given below.

Before leaving the SHB, some results are presented in which stress measurements were attempted in tamped configurations to demonstrate the ability of the SHB to measure long duration stresses of very low amplitude.

6.1.5 Tamped and Long Duration Stresses. An attempt to tamp 3DQP blow-off gave the result shown in Figure 18 (Shot 6057). The tamper (carbon cloth plus 0.020-inch Be) failed to contain the blow-off material completely. But note the wider pulse for 3DQP than that shown in Figure 15 for an untamped 3DQP specimen. [Note also that the stress wave reflected from the rear end of the bar arrives (inverted) back at the crystal after about 120  $\mu$ s, as is seen on the slow sweep trace.]



2 Volts/div.  
149 bars/div.  
20  $\mu$ s/div.  
 $\frac{1}{2}$  Volt/div.  
37.3 bars/div.  
10  $\mu$ s/div.

Time →

Figure 18. SHB result for partially tamped 3DQP. GAMBLE I  
Shot no. 6057. Quartz crystal in aluminum rods.  
Tamper: carbon cloth plus 0.020 inch beryllium.

Although not stated earlier, Shot No. 6046 with phenolic resin shown in Figure 17, also includes a tamper in front of the resin. The tamper, 0.020-inches thick ATJ graphite, could only extend the stress duration and hence does not alter the conclusions stated above regarding the pulse tail amplitude. Note that the main pulse is again somewhat wider, nearly 15  $\mu$ s, than other main pulses shown as a result of the partial tamping. Several other tamper configurations

were tried, but because of the short range of the low mean energy electrons, a tamper could not be made thick enough to prevent rupture by the blown-off material.

In order to demonstrate the ability of the SHB to actually record a very long duration low amplitude stress, a shot was made with low density carbon foam on the front of the rod. This foam absorbed the electrons fully without generating any significant measurable stress. However, a late-time stress was expected at about 60  $\mu$ s, due to arrival of material from vaporization of the Mylar anode. The results are shown in Figure 19, Shot No. 6063. A compressive stress in this shot is represented by a positive voltage (the voltage sign changed from shot to shot depending upon the lead connections). At 60 to 70  $\mu$ s, a low amplitude, long duration stress arrived which reached 1.5 bars peak. Note the early time noise of about 8 mV, equivalent to about 0.3 bars, is in agreement with the noise of Shot 6040, shown in Figure 14. In Shot 6040 (Fig. 14) anode debris was prevented from reaching the SHB by the spaced-off absorber, so no late time stress was observed. In other specimen shots, the anode debris was prevented from reaching the SHB by the blown-off 3DQP or phenolic resin material. This Shot (No. 6063, Fig. 19) demonstrates the ability of the SHB to record low amplitude (few bars) stresses for long times in an electron-beam environment.

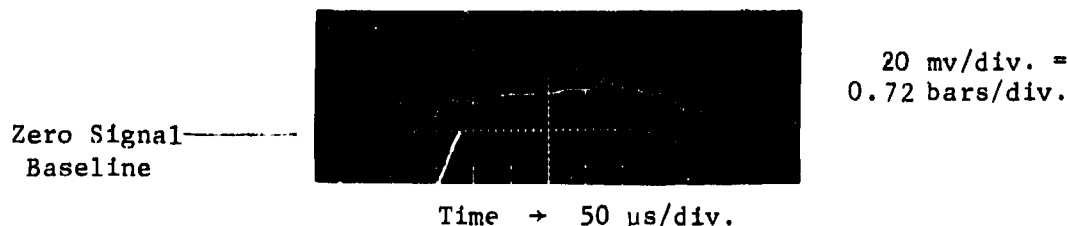


Figure 19. SHB measurement of long, low stress from anode debris.  
GAMBLE I Shot No. 6063. Quartz crystal in Plexiglas rod.

## 6.2 One-Dimensional CMX Gauge Results

This new gauge type is discussed in Section 5.2. It was tested using both the REHYD and Blackjack 3 accelerators. Many shots were made to (1) minimize the noise levels, (2) study the effect of circuit capacitance, (3) learn the necessity of crow-barring the cables until after shot time, and (4) discover the advantages gained by use of the line-drivers (discussed in Section 5.1) for effectively eliminating the long (100 foot) cable run between the gauge and the

recording oscilloscopes. These tests were also used to extensively check out the signal conditioning electronics for later use in the underground test.

In order to verify the gauge output, simultaneous measurements of the stress pulse were made with a laser velocity interferometer. The interferometer monitored the displacement of the rear crystal surface by using light reflected from the rear electrode coating on the crystal. Figure 20 shows the successful results recorded for a CMX gauge behind a one-half inch thick 3DQP sample, with a one-inch Plexiglas backing. Included on the figure is the reduced laser interferometer result. The CMX data were reduced to stress using the known X-cut quartz crystal piezoelectric coefficient. It is seen that the pulse amplitudes and shapes are in excellent agreement. The laser data terminates on the back side of the pulse due to light loss, a not uncommon occurrence with composite materials since the surface can tilt locally on a scale the size of the focused laser spot. The CMX gauge output was recorded for longer than 20  $\mu$ s, the first 2  $\mu$ s of which are shown in Figure 20. Figure 21 shows the gauge output, on a slower sweep, for 7  $\mu$ s past the peak. The stress does not remain at zero for two reasons. First, the QP is backed by Plexiglas, and the acoustic impedance difference between the two materials caused a reflected (tensile) wave to travel back into the QP. The amplitude of this reflected wave is 28% of the stress amplitude incident at the interface. Second, the electron beam that irradiated the QP surface was not spatially uniform, causing non-uniform blow-off (Fig. 22). This nonuniform loading results in a shortened time for which one-dimensional strain exists at the crystal. Similar nonuniform loading was encountered with the beams at both REHYD and Blackjack 3. Unfortunately, it was necessary to install a new diode insulator on the BJ3 to improve the rather erratic machine performance. This operation could not be included in our schedule, and hence the present test series had to be terminated.

However, the successful application of the charge-mode crystal in a one-dimensional strain geometry has been demonstrated. A very low noise level (less than one-bar) and excellent agreement with laser interferometry were both obtained. The gauge can now be used for long duration (>10  $\mu$ s) stress recording with a 20 ns time resolution over the complete stress history, including the main stress pulse as well as any low amplitude tail. It is only necessary that the following conditions be met:

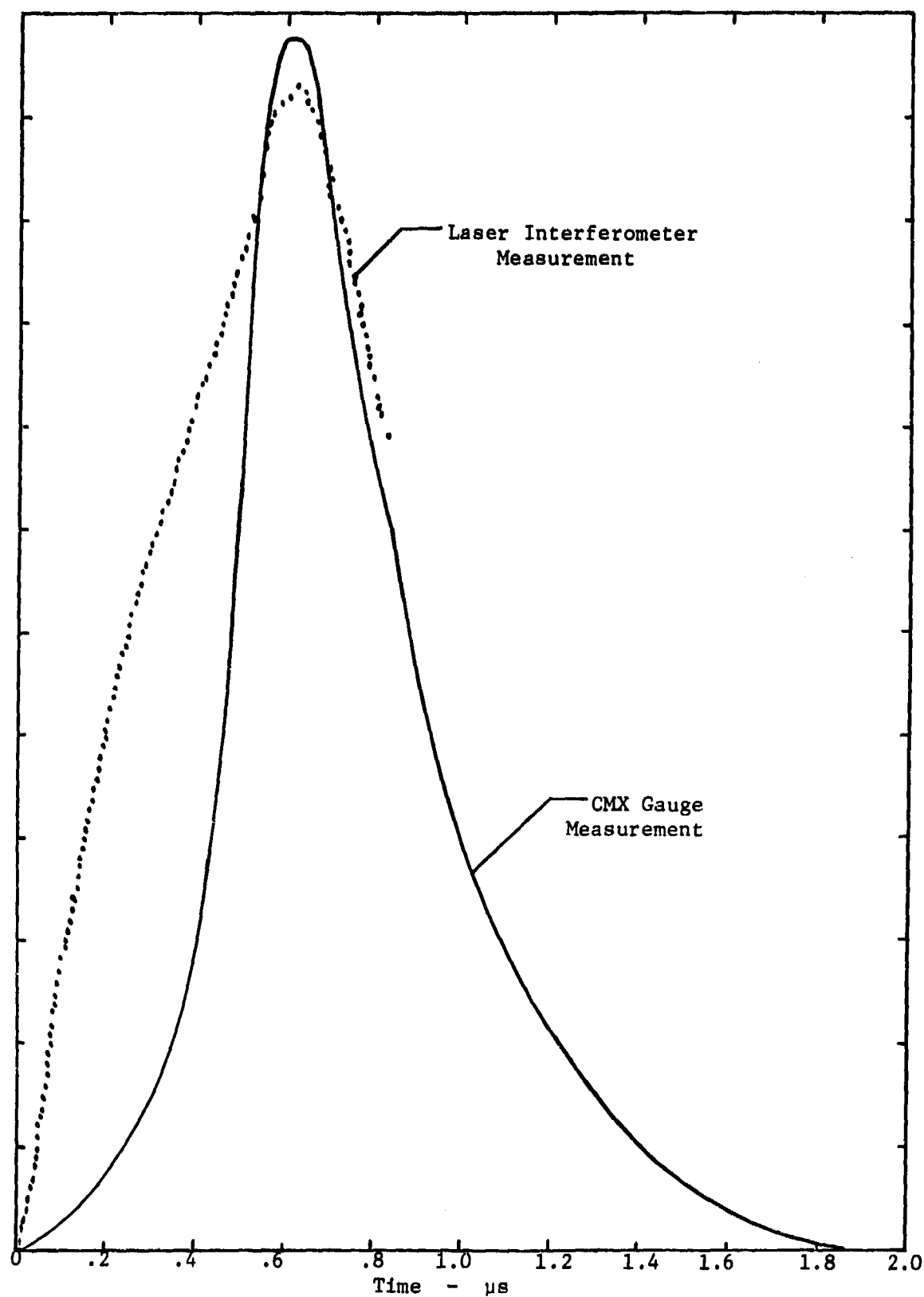


Figure 20. CMX result on 3DQP. REHYD Shot No. 2122. Laser Interferometer result and PUFF hydrocode calculation shown for comparison.

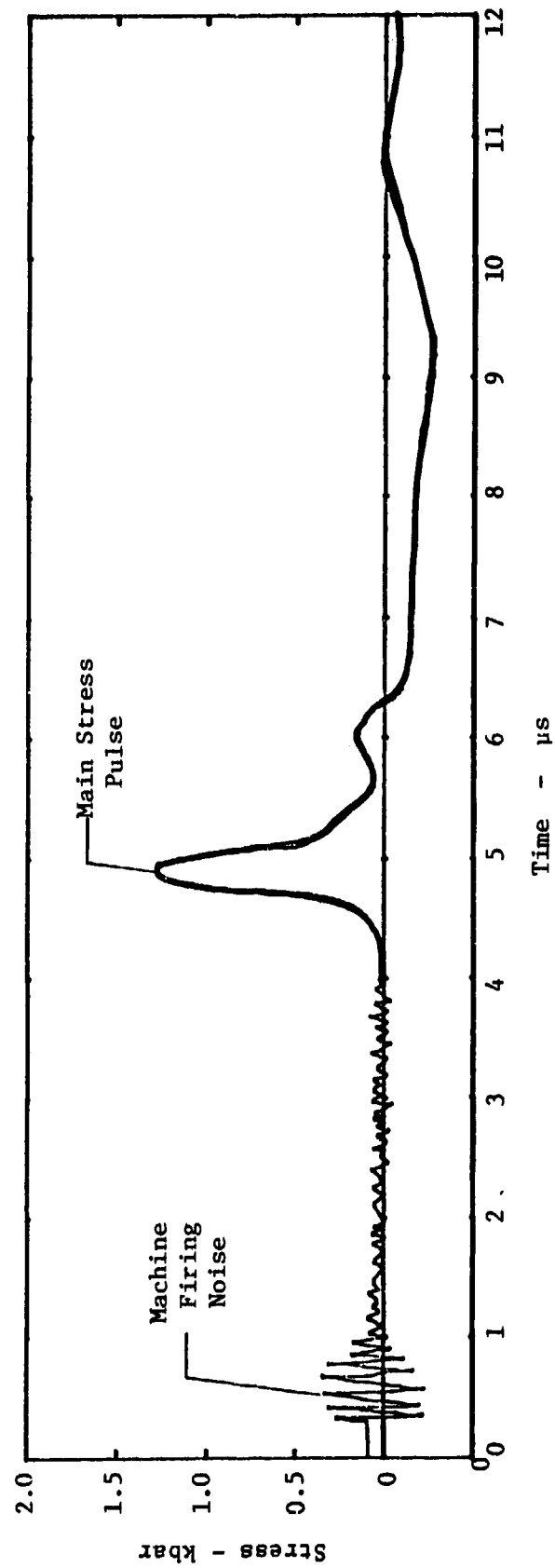


Figure 21. CMX result on 3DQP. REHYD Shot No. 2122. Long time data record.

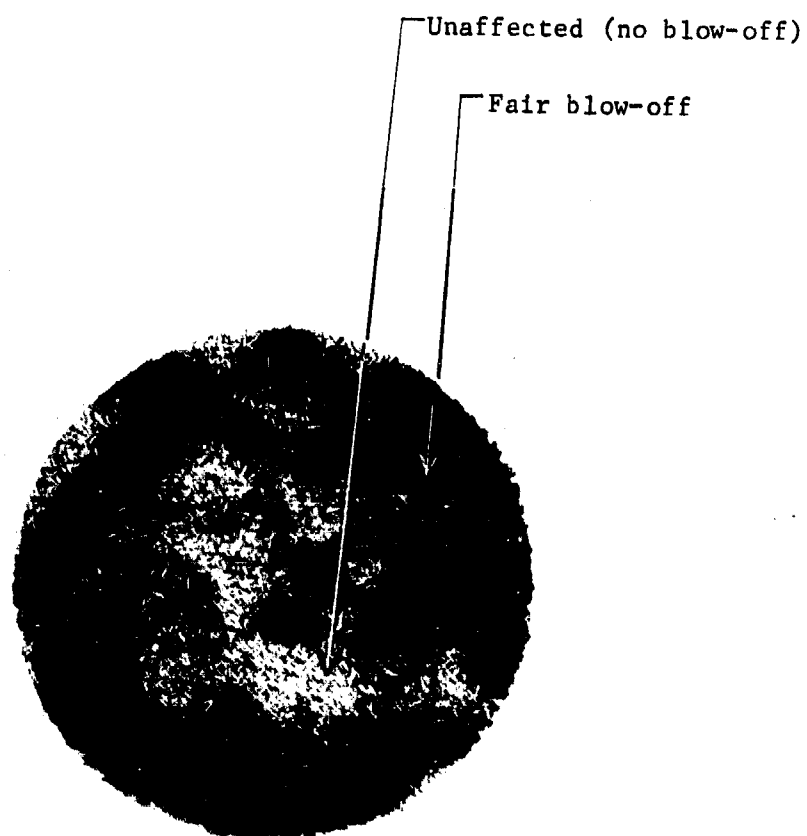


Figure 22. Photograph of Irradiated quartz phenolic target showing non-uniform blow-off. Blackjack 3 shot no. 2122.

- (a) The backing material have essentially the same acoustic impedance as the specimen. This condition is readily satisfied by using specimen material for the backing; the gauge is then a true "in-material" gauge.
- (b) The electron beam must be uniform over a radius given by the desired stress recording time multiplied by the wave speed in the specimen.
- (c) The circuit capacitance be adjusted for the desired voltage output, not to exceed the line driver capabilities. If necessary, other piezoelectric materials (e.g.,  $\text{LiNbO}_3$ ) may be substituted for the quartz for greater sensitivity.

### 6.3 Discussion of Preliminary Underground SHB Test Results

Two Split-Hopkinson Bars were used to study UGT induced stresses from 3DQP blow-off. These SHB's used half-inch diameter fused silica rods: 6 inches long front rod (26  $\mu\text{s}$  transit time), and 10 inch long back rod (85  $\mu\text{s}$  double transit time). Both gauges were located in prime exposure space, but for one gauge, the background gauge, the 3DQP was shielded by a totally stopping absorber mounted over the the collimator on the end of the cassette. Post-shot recovery showed that the QP stayed on both rods, and that indeed the QP in the normal gauge had been irradiated and "fluffed-out", whereas the QP on the background gauge showed no radiation (or any other) damage.

The SHB outputs were fed by coaxial cable into Ktech line-drivers located in an alcove. The signals were recorded on oscilloscopes a few thousand feet from the alcove, and were cable compensated for attenuation of the high frequencies. The oscilloscope records were digitized (Figure 23) and converted to stress at the gauge (Figure 24). The large pulses on the records represent stresses, but they are not from the QP blow-off. That it is a stress is proven by the fact that on a slow oscilloscope sweep the pulse is seen (highly attenuated) to reflect from the rear of the backup rod. This pulse is most likely due to a shock generated in the absorbing collimator, which pulse would be similar for both gauges. We had attempted to minimize its coupling to the SHB with the use of a low-density polyurethane foam, and of course, the rods are isolated from the cassette by rubber "O" rings. This pulse could be eliminated in the future by spatially isolating the collimator from the SHB cassette. This pulse is definitely not the QP pulse because (1) it is on the background

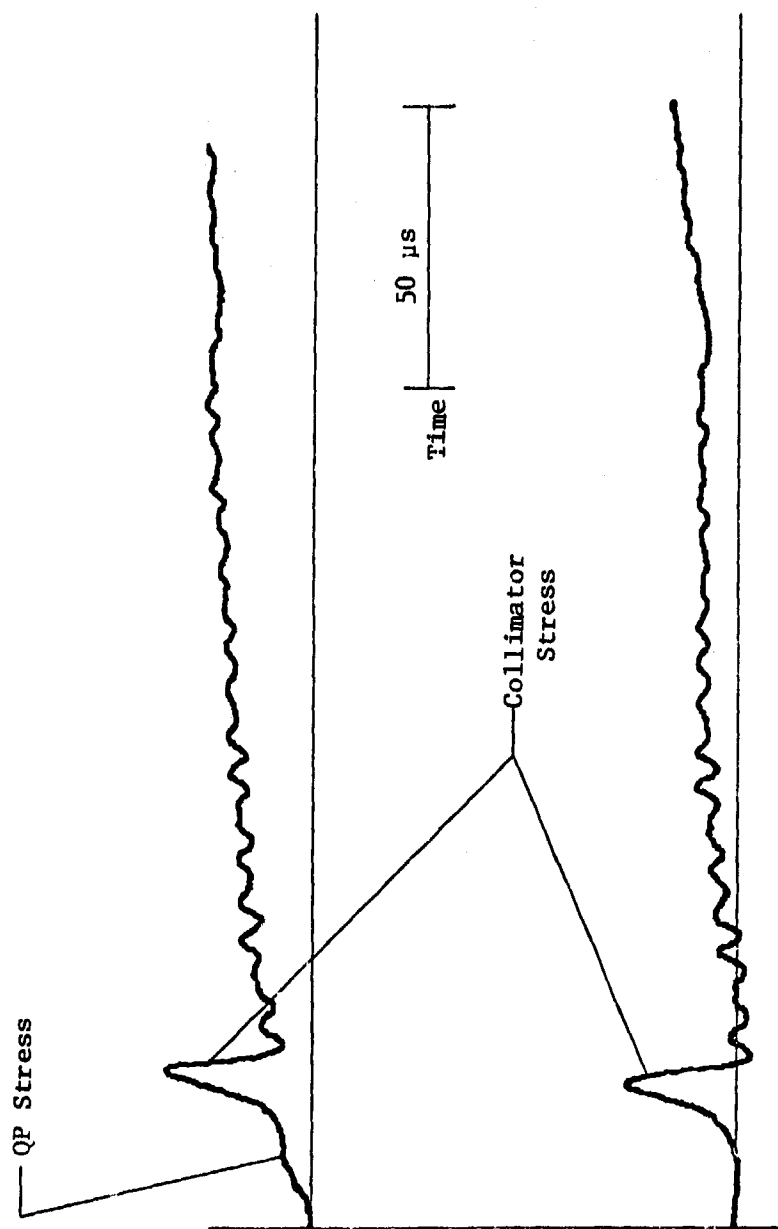


Figure 23. SHB results from underground test. (a) Active and (b) Background results

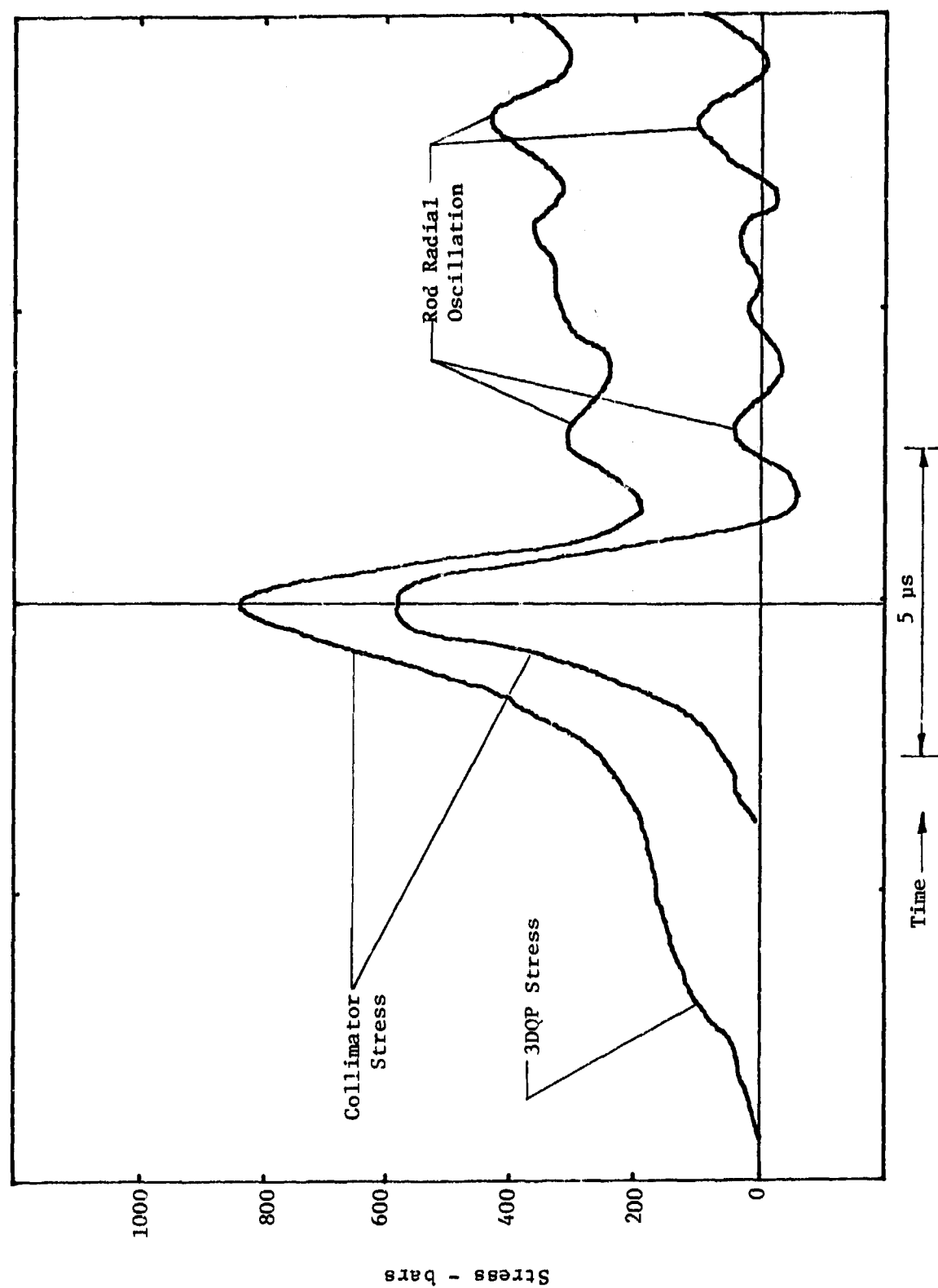


Figure 24. SHB results from underground test. Comparison of (a) active and (b) background results.

gauge, and (ii) it arrives at the crystal too late: at 40  $\mu\text{s}$  rather than at 32  $\mu\text{s}$  when the QP pulse is known to arrive. The timing was as follows: 6  $\mu\text{s}$  shock transit through the QP, plus 26  $\mu\text{s}$  transit time down the 6-inch fused silica front rod, giving a total of 32  $\mu\text{s}$  until the QP stress arrived at the quartz charge-mode gauge. The scopes were triggered at about 26  $\mu\text{s}$  after zero time, so the pulse from the QP arrives at the gauge 6  $\mu\text{s}$  after start of the oscilloscope sweep, where it is seen on the active gauge record. The QP stress pulse of interest is the leading "foot" of the pulse on the active gauge (see Figures 23 and 24). The noise level before the stress peak is very low, and is equivalent to less than 10 bars. It can easily be made even less by using the more sensitive lithium niobate instead of quartz. The oscillations after the stress peak are also without noise; they are due to radial oscillations of the rod. This can easily be seen by noting the nearly exact similarity in the oscillations in the active and background gauges.

Subtracting the background gauge record from the active gauge record up until the time of the collimator induced pulse gives the QP stress transmitted down the rod. The resulting QP stress pulse, shown in Figure 25, has a peak of 200 bars and a width of about 15  $\mu\text{sec}$ . The area under this pulse is 1.4 ktaps, giving a total momentum over the rod area of  $1.77 \times 10^3$  dyne-sec. Because the acoustic impedance of fused silica ( $1.3 \text{ gm cm}^{-2} \mu\text{s}^{-1}$ ) is greater than that of 3DQP (0.52), the stress wave in the QP partially reflects from the QP/fused silica interface as a compressive wave. This causes a momentum enhancement of 40% transmitted (by the first main pulse) into the SHB rod. Thus the  $1.77 \times 10^3$  dyne-sec measured prompt impulse at the gauge, represents a 3DQP prompt impulse of 1.26 dyne-sec. Dividing by the observed 3DQP blow-off area (1.0 cm diameter  $\Rightarrow 0.79 \text{ cm}^2$ ) gives 1.52 ktaps for the 3DQP blow-off momentum per unit area. This prompt impulse can be used to compare with the results from the other 3DQP stress pulse tail experiment gauges measuring the total late time impulse. The results agree well. Even though the stress pulse attenuates and broadens as it propagates down the rod, momentum is conserved. Finally, the slow rise seen on the records following the "collimator" pulse, is attributed to structural oscillation of the entire SHB cassettes. It has been established by means of extensive laboratory tests, that this "drift" is not electronic in nature caused by either the line-drivers or the oscilloscopes. In the future, for

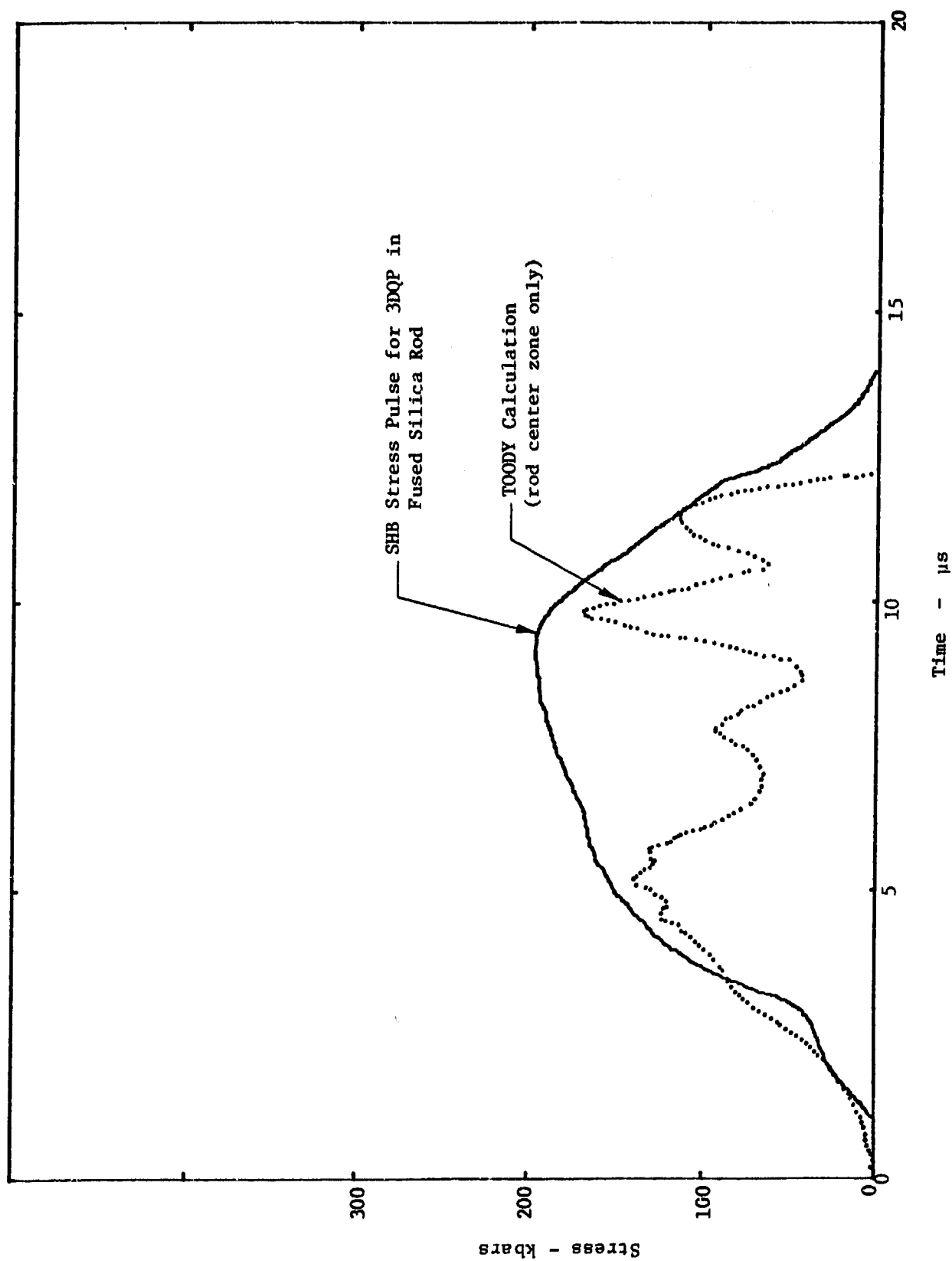


Figure 25. SHB stress pulse for 3DQP from underground test and comparison with two-dimensional hydrodynamic calculation.

longer time recording, the SHB cassettes should be inertially isolated from the bulkhead. Because of this spurious motion, the amplitude of any pulse tail stress cannot be determined from these data with a resolution better than about 100 bars. These underground tests results may be summarized briefly as follows:

1. The SHB has worked very successfully in UGT for the first time: a stress history has been measured for several tens of microseconds. The noise level before the stress arrival was very low--less than 10 bars--enabling any stress levels of interest to be recorded. High quality SHB data can be easily obtained in UGT tests.
2. The measured stress amplitude and duration, and prompt impulse agreed well with pre-test predictions and with other related measurements.
3. In the future the SHB cassette should be completely shock isolated from its collimator and inertially isolated from the bulkhead if recording longer than 40  $\mu$ s is required.

## SECTION 7

### REFERENCES

1. Keller, D. V., Brooks, A. L. and Jenrette, B. D., "Split-Hopkinson Bar Development for Underground Testing", Ktech Corp. TR76-02, April 1976.
2. Schallhorn D., Oswald R., Skillington G., Oldham, T., "Some Characteristics of the GAMBLE I Electron Beam", Harry Diamond Laboratories, Washington, D. C. Report HDL-TR-1977, December 1974.
3. Schuch R. and Woodall H., "REHYD Development and Installation Report", Sandia Laboratories Report No. SAND77-0599, December 1977.
4. Phelps, D. and Rauch, J., "Description of Blackjack 3 and Blackjack 3 Prime", Maxwell Laboratories Report MLR-748, May 1978.
5. "ELTRAN: One-Dimensional Monte Carlo Electron transport Code", Sandia Laboratories Report SL-TM-68-713, Radiation Shielding Information Center, January 1969.
6. "PUFF-74: A Material Response Computer Code", Robert Cecil, C. David Newlander, Capt Richard J. Scammon, Air Force Weapons Laboratory, Kirtland AFB, NM, Report No. AFWL-TR-76-43, January 1977.
7. Anderson, E., "EDEP Code for Predicting Radiant Energy Deposition, Ktech Corporation Report SB73-2, August 1973.
8. Langley, R. W., "Analytical Relationships for Estimating the Effects of X-rays on Materials", Air Force Rocket Propulsion Laboratory, Edwards, CA Report No. AFRPL-TR-74-52, September 1974.
9. Swegli, J. "TOODY: A Computer Program for Two-dimensional Wave Propagation," Sandia Laboratories Report No. SAND-78-0552, September 1978.

## DISTRIBUTION LIST

### DEPARTMENT OF DEFENSE

Assistant to the Secretary of Defense  
Atomic Energy

ATTN: Executive Assistant

Defense Advanced Rsch. Proj. Agency  
ATTN: TIO

Defense Technical Information Center  
12 cy ATTN: DD

Defense Intelligence Agency  
ATTN: DT-2

Defense Nuclear Agency

ATTN: SPSS

ATTN: STSP

ATTN: SPTD

ATTN: SPAS

ATTN: DDST

4 cy ATTN: TITL

Field Command

Defense Nuclear Agency

ATTN: FCPR

ATTN: FCTMD

Field Command

Defense Nuclear Agency

Livermore Division

ATTN: FCPRL

Joint Chiefs of Staff

ATTN: J-5, Nuclear Division

ATTN: SAGA/SFD

ATTN: J-5, Force Planning & Program Div.

ATTN: SAGA/SSD

Joint Strat. Tgt. Planning Staff

ATTN: JPTM

ATTN: JLTW-2

Undersecy. of Def. for Rsch. & Engrg.

Department of Defense

ATTN: Strategic & Space Systems (OS)

### DEPARTMENT OF THE ARMY

BMD Advanced Technology Center

Department of the Army

ATTN: ATC-T, M. Capps

Program Manager

BMD Program Office

Department of the Army

ATTN: Technology Division

BMD Systems Command

Department of the Army

ATTN: BMDSC-H, N. Hurst

Deputy Chief of Staff for Ops. & Plans

Department of the Army

ATTN: DAMO-NCZ

### DEPARTMENT OF THE ARMY (Continued)

Deputy Chief of Staff for Rsch. Dev. & Acq.  
Department of the Army

ATTN: DAMA-CSS-N

Harry Diamond Laboratories

Department of the Army

ATTN: DELHD-N-P, J. Gwaltney

ATTN: DELHD-N-RBC, D. Schallhorn

ATTN: DELHHD-N-P

U.S. Army Ballistic Research Labs

ATTN: DRDAR-BLV, W. Schuman, Jr.

ATTN: DRDAR-BLE, J. Keefer

ATTN: DRDAR-BLV

U.S. Army Material & Mechanics Rsch. Ctr.

ATTN: DRXMR-HH, J. Dignam

U.S. Army Materiel Dev. & Readiness Cmd.

ATTN: DRCDE-D, L. Flynn

U.S. Army Missile R&D Command

ATTN: DRDMI-TKP, W. Thomas

U.S. Army Nuclear & Chemical Agency

ATTN: Library

U.S. Army Research Office

ATTN: Technical Library

### DEPARTMENT OF THE NAVY

Naval Research Laboratory

ATTN: Code 6770, G. Cooperstein

ATTN: Code 2627, Tech. Library

ATTN: Code 7908, A. Williams

Naval Sea Systems Command

ATTN: SEA-0351

ATTN: SEA-0352, M. Kinna

Naval Weapons Evaluation Facility

ATTN: L. Oliver

Office of the Chief of Naval Operations

ATTN: 604E14, R. Blaise

ATTN: Op-981

ATTN: Op-604C

Strategic Systems Project Office

Department of the Navy

ATTN: NSP-273

ATTN: NSP-272

Naval Surface Weapons Center

White Oak Laboratory

ATTN: Code K06

ATTN: Code R15, J. Petes

ATTN: Code K06, C. Lyons

ATTN: Code F31

DEPARTMENT OF THE AIR FORCE

Aeronautical Systems Division, AFSC  
ATTN: ASD/ ENFTV

Air Force Materials Laboratory  
ATTN: MBC, D. Schmidt  
ATTN: MBE, G. Schmitt  
ATTN: LLM, T. Nicholas

Air Force Rocket Propulsion Laboratory  
ATTN: LKCP, G. Beale

Air Force Systems Command  
ATTN: XRTO  
ATTN: SOSS

Air Force Weapons Laboratory  
ATTN: DYS  
ATTN: DYV  
ATTN: NT  
ATTN: DYT  
ATTN: SUL

Deputy Chief of Staff  
Research, Development, & Acq.  
Department of the Air Force  
ATTN: AFRDQSM  
ATTN: AFRD

Foreign Technology Division  
Air Force Systems Command  
ATTN: TQTD  
ATTN: SDBS, J. Pumphrey  
ATTN: SDBG

Headquarters Space Division  
Air Force Systems Command  
ATTN: DYS

Ballistic Missile Office  
Air Force Systems Command  
ATTN: MNNR  
ATTN: MNNH

Headquarters Space Division  
Air Force Systems Command  
ATTN: RSMA  
ATTN: RSS  
ATTN: RSSE

Strategic Air Command/XPFS  
Department of the Air Force  
ATTN: XPQM  
ATTN: XPFS  
ATTN: DOXT  
ATTN: XOBM

DEPARTMENT OF ENERGY

Department of Energy  
ATTN: Doc. Con. for OMA/RD&T

DEPARTMENT OF ENERGY CONTRACTORS

Lawrence Livermore Laboratory  
University of California  
ATTN: Doc. Con. for L-92, C. Taylor  
ATTN: Doc. Con. for L-125, J. Keller  
ATTN: Doc. Con. for D. Hanner  
ATTN: Doc. Con. for L-96, L. Woodruff

Los Alamos Scientific Laboratory  
ATTN: Doc. Con. for R. Skaggs  
ATTN: Doc. Con. for J. McQueen/J. Taylor  
ATTN: Doc. Con. for D. Shover  
ATTN: Doc. Con. for R. Dingus

Sandia Laboratories  
Livermore Laboratory  
ATTN: Doc. Con. for T. Gold  
ATTN: Doc. Con. for H. Norris, Jr.

Sandia Laboratories  
ATTN: Doc. Con. for M. Cowan  
ATTN: Doc. Con. for C. Mehl  
ATTN: Doc. Con. for C. Broyles

DEPARTMENT OF DEFENSE CONTRACTORS

Acurex Corp.  
ATTN: J. Huntington

Aerospace Corp.  
ATTN: R. Crollius  
ATTN: R. Mortensen  
ATTN: W. Mann  
ATTN: R. Strickler

Avco Research & Systems Group  
ATTN: W. Broding  
ATTN: J. Gilmore  
ATTN: P. Grady  
ATTN: J. Stevens  
ATTN: G. Weber  
ATTN: Document Control

Battelle Memorial Institute  
ATTN: M. Vanderlind

Boeing Co.  
ATTN: B. Lempriere

California Research & Technology, Inc.  
ATTN: K. Kreyenhagen

Effects Technology, Inc.  
ATTN: R. Parrise/M. Rosen  
ATTN: R. Wengler/R. Bick

Ford Aerospace & Communications Corp.  
ATTN: P. Spangler

General Electric Co.  
Space Division  
ATTN: G. Harrison  
ATTN: D. Edelman

DEPARTMENT OF DEFENSE CONTRACTORS (Continued)

General Electric Co.  
Re-Entry & Environmental Systems Div.  
ATTN: P. Cline

General Electric Company-TEMFO  
ATTN: DASIAC

General Research Corp.  
Santa Barbara Division  
ATTN: R. Rosenthal

Institute for Defense Analyses  
ATTN: Classified Library  
ATTN: J. Bengston

Ion Physics Corp.  
ATTN: R. Evans

Kaman Avidyne  
Division of Kaman Sciences Corp.  
ATTN: R. Ruetenik

Kaman Sciences Corp.  
ATTN: R. Sachs/R. O'Keefe  
ATTN: F. Shelton  
ATTN: T. Meagher

KTech Corp.  
ATTN: D. Keller  
ATTN: D. Rice

Lockheed Missiles & Space Co., Inc.  
ATTN: O. Burford  
ATTN: R. Walls

Lockheed Missiles and Space Co., Inc.  
ATTN: F. Borgardt

Lockheed Missiles and Space Co., Inc.  
ATTN: T. Fortune

Martin Marietta Corp.  
Orlando Division  
ATTN: L. Kinnaird

TRW Defense & Space Sys. Group  
San Bernardino Operations  
ATTN: L. Berger  
ATTN: V. Blankenship  
ATTN: W. Polich

DEPARTMENT OF DEFENSE CONTRACTORS (Continued)

McDonnell Douglas Corp  
ATTN: L. Cohen  
ATTN: H. Berkowitz  
ATTN: M. Schneider  
ATTN: J. Peck

Pacific-Sierra Research Corp.  
ATTN: G. Lang

Physics International Co.  
ATTN: J. Shea

Prototype Development Associates, Inc.  
ATTN: J. McDonald  
ATTN: N. Harington

R & D Associates  
ATTN: W. Graham, Jr.  
ATTN: P. Rausch  
ATTN: C. MacDonald  
ATTN: F. Field

Rand Corp.  
ATTN: R. Rapp

Science Applications, Inc.  
ATTN: O. Nance  
ATTN: W. Yengst

Science Applications, Inc.  
ATTN: W. Seebaugh  
ATTN: W. Layson

Southern Research Institute  
ATTN: C. Pears

SRI International  
ATTN: H. Lindberg  
ATTN: D. Curran  
ATTN: G. Abrahamson

Systems, Science & Software, Inc.  
ATTN: T. McKinley  
ATTN: G. Gurtman  
ATTN: R. Duff

Terra Tek, Inc.  
ATTN: S. Green

TRW Defense & Space Sys. Group  
ATTN: J. Farrei  
ATTN: W. Wood  
2 cy ATTN: P. Dai/D. Jortner